Aus der

Orthopädischen Universitätsklinik mit Poliklinik Tübingen

Changes in stiffness of the extracellular and pericellular matrix of chondrocytes in human articular cartilage in the course of osteoarthritis

Inaugural-Dissertation
zur Erlangung des Doktorgrades
der Medizin

der Medizinischen Fakultät
der Eberhard-Karls-Universität
zu Tübingen

vorgelegt von

Jacobi, Leonhard Felix

2023

Dekan: Professor Dr. B. Pichler

1. Berichterstatter: Professor Dr. U. Hofmann
2. Berichterstatter: Professor Dr. J. Kolbenschlag

Tag der Disputation: 11.04.2023

I Table of content

II List of figures

III List of tables

IV List of equations

V Abbreviations

ACI	Autologous chondrocyte implantation
ADAMTSs	A disintegrin and metalloproteinase with thrombospondin motifs
AFM	Atomic force microscopy/microscope
BC	Big cluster
BSA	Bovines serum albumin
DAPI	4′,6-diamidino-2-phenylindole
DMEM	Dulbecco's modified Eagle's medium
DS	Double string
ECM	Extracellular matrix
GAGs	Glycosaminoglycans
ICRS	International Cartilage Repair Society
LIF	Leukemia inhibitory factor
MMPs	Matrix metalloproteinases
MRI	Magnetic resonance imaging
NSAIDs	Nonsteroidal anti-inflammatory drugs
OA	Osteoarthritis
PCM	Pericellular matrix
PGs	Proteoglycans
SC	Small cluster
SCSO	Superficial chondrocyte spatial organization
SS	Single string
TNF	Tumor necrosis factor
YM	Young’s modulus

VI Abstract

Osteoarthritis (OA) is the most common joint pathology of adults worldwide, characterized by degeneration and progressive loss of articular cartilage. Articular cartilage covers the distal ends of bones within a joint and facilitates load transmission and shock absorption. Further, it decreases friction between the joint surfaces during movement and minimizes exerted forces on the underlying subchondral bone. Articular cartilage is an avascular connective tissue without blood supply, lymphatic vessels, or neural innervation. These anatomical characteristics explain its limited regenerative capability, which contributes to the onset and progression of OA, characterized by tissue degeneration of cellular and extracellular cartilage components.

Chondrocytes constitute the sole cartilage cell type. Their primary function is to synthesize and maintain the extracellular matrix (ECM), which is the major component of the articular cartilage. The ECM is comprised of structural proteins of the collagen and proteoglycan family responsible for the biomechanical properties of the articular cartilage. The pericellular matrix (PCM) represents a distinct subtype of ECM. It is a thin layer of a highly specialized matrix that directly surrounds the chondrocyte. While a high abundance of the fibrous protein collagen type II characterizes the ECM, the PCM predominantly contains collagen type VI and the proteoglycan perlecan. During the onset and progression of OA, degradative processes triggered by chondrocytic dysregulation lead to structural and biomechanical alterations in the ECM and PCM. Microscopic studies have shown that changes in spatial chondrocyte organization are a salient feature of the OA pathogenesis.

Further, OA is characterized by a dysregulation in the amount and distribution of the collagen proteins in the ECM; while the collagen type II concentration decreases, collagen type I can be found in increased abundance. The OA-related collagen remodeling seems to affect the structural and biomechanical properties of the ECM. The alteration in the biomechanical properties of the articular cartilage is a hallmark of degenerative OA and results in decreased resistance to compressive and shear forces.

The present study aimed to investigate the cartilage tissue stiffness of the ECM and PCM by means of atomic force microscopy (AFM) in patients with different clinical stages of degenerative knee OA. AFM is a technique that enables the investigation of biomechanical properties and topography of cartilage tissue. In the present study, AFM was used to investigate the cartilage surface stiffness in regions of the ECM and PCM using spatial chondrocyte organization as an image-based biomarker to grade the severity of local OA-related tissue degeneration in human articular cartilage. Further, immunofluorescence labeling of ECM components (collagen type I and II) was conducted to qualitatively assess osteoarthritic degenerative changes regarding spatial chondrocyte organization. The AFM analysis was combined with immunofluorescence labeling of the cartilage samples to provide information on the relationship between matrix stiffness changes and structural protein alterations.

The main findings of the present study were that as OA degeneration of cartilage occurred (as defined by changes in spatial chondrocyte organization), the ECM and PCM stiffness showed a distinct and linear decrease. In healthy cartilage areas, represented by chondrocyte organization in single strings (SS), the stiffness for both ECM and PCM was the highest (with the ECM being higher than the PCM). With the onset of OA, as indicated by the presence of double strings (DS) and in further advanced stages by small clusters (SC), the ECM and PCM stiffness decreased continuously. The stiffness was the lowest as chondrocytes were organized as big clusters (BC), indicating late stages of OA.

Immunofluorescence staining illustrated continuous changes in the abundance and distribution of collagen type I and collagen type II in the ECM during OA onset and progression. A reduction in collagen type II and an increase in collagen type I staining was noted along the progression of OA that corresponded with a continuous cartilage stiffness reduction of both matrices. The observed staining signal reduction of collagen type II and the increase of collagen type I was most prominent as spatial chondrocyte organization changed from double strings to small clusters.

The present study is the first to describe stiffness changes of the ECM and PCM in relation to changes in spatial chondrocyte organization. From the study findings, it can be hypothesized that OA-related cartilage damage manifests itself in a dysfunctional synthesis of collagen type II. It can also be speculated that the rearrangement in chondrocyte spatial organization and the impairment of the articular cartilage biomechanical function is partly of secondary effect to a reduction in collagen type II quantity and quality.

1. Introduction

Osteoarthritis (OA), also known as degenerative joint disease, is the most common form of arthritis worldwide and mainly affects the elderly population. OA is characterized by progressive degeneration and, ultimately, loss of articular cartilage of the joint. This degenerative disease affects millions of people worldwide and causes a severe reduction of life quality as it causes chronic pain and restricts joint mobility. The physical disability of the patients causes a significant socio-economic burden, which highlights the need for improved therapeutic and diagnostic strategies (Hassanali and Oyoo, 2011, Palazzo et al., 2016, Heidari, 2011).

Initially, OA was viewed as simply a manifestation of age-related tissue deterioration. However, today OA is recognized as a complex multifactorial degenerative joint disease induced by several interrelated components, including biochemical, biomechanical, metabolic, biomedical, and genetic factors. Such factors contribute to OA-related degeneration and progressive loss of articular cartilage, which leads to pain and disability (Wilusz et al., 2013, Man and Mologhianu, 2014, Hassanali and Oyoo, 2011). OA is recognized as a whole-joint disease with complex pathomechanisms that involve multiple joint structures. Apart from cartilage, affected structures include periarticular muscles, ligaments, joint capsule, synovial membrane, and subchondral bone (Peters et al., 2018, Hunter and Felson, 2006, Man and Mologhianu, 2014).

The pathomechanism of the onset and progression of OA is only partly understood, which is one reason for the lack of targeted therapy options that could slow down the progression of degenerative processes or even restore damaged cartilage (Chen et al., 2017a). In the early OA stages, non-surgical therapies are advised. However, conservative therapy approaches are often insufficient in progressed stages of OA, and symptoms cannot be controlled anymore. In this case, surgical interventions such as total knee replacement can be recommended to the patient.

A better understanding of the pathomechanisms of osteoarthritic degenerative processes might hold critical information to further develop therapeutic and diagnostic strategies. Early detection and prevention of OA might also be possible if biomechanical and structural cartilage changes occurring at the OA onset are understood in more detail.

1.1. Anatomy of the knee joint

The knee joint is a hinge-type synovial joint that establishes the connection between the femur, tibia, fibula, and the posterior surface of the patella. Besides bony components (femur, tibia, fibula, and patella), the knee joint comprises articular cartilage, menisci, ligaments, tendons, bursae, and a joint capsule with a synovial membrane (Hirschmann and Müller, 2015, Oliveira and Lu, 2017). The knee joint consists of various articulations. These include the tibiofemoral articulation, which consists of the articulating surfaces of the femoral condyles and the tibial plateau. The patellofemoral joint consists of the patella surface found at the distal metaphysis of the femur and the posterior surface of the patella. The fibula is in contact with the lateral side of the proximal tibia and thereby constitutes the tibiofibular joint (Saavedra et al., 2012, Fox et al., 2009, Flandry and Hommel, 2011). Together, these articulations allow an extension of 5-10°and a 120-150° flexion, which is the primary movement of the knee joint. Besides, internal rotation of 10° and external rotation of 30-40° is possible in the flexed knee (Saavedra et al., 2012). This range of actions enables the knee joint to promote stability and control during movement (Oliveira and Lu, 2017).

In the knee joint, articular cartilage covers the joint surfaces where the femur, tibia, fibula, and the posterior surface of the patella articulate. Articular cartilage mainly functions in decreasing friction between bony joint structures. Besides, when the knee joint is exposed to dynamic forces, articular cartilage plays a significant role in shock absorption. (Abulhasan and Grey, 2017, Fox et al., 2009). The medial and lateral menisci of the knee joint provide stability for the femorotibial articulation and they also play an important role in shock absorption.

In addition, they are essential for axial load distribution and joint lubrication, and they provide nutrition to the knee joint (Fox et al., 2012).

Ligaments, which attach bone to bone, and tendons, which connect bone to muscle, are essential for strength, movement, and stabilization of the knee joint. Tendons guide and assist muscular functions, and ligaments prevent bone movement which exceeds the normal range of motion. Another vital structure that surrounds the knee joint is the articular capsule. It consists of a fibrous capsule and a synovial membrane. The fibrous capsule protects the joint space and provides further stability as it restricts excessive movement (Oliveira and Lu, 2017, Jung et al., 2009). The synovial membrane lines the fibrous capsule and secretes synovial fluid crucial for cartilage surface lubrication. The synovial fluid also provides oxygen and nutrients to the articular cartilage and menisci (Fox et al., 2009, Travascio and Jackson, 2017). The interplay between all the above-discussed anatomical structures is essential for the knee joint to perform its complex mechanical functions (Hirschmann and Müller, 2015).

1.2. Function and structure of articular cartilage

1.2.1. Composition of articular cartilage

Articular cartilage is a specialized connective tissue that reduces friction in the joint as it provides a smooth surface for articulation. It also functions in shock absorption during movement as it governs load transmission to subjacent bone structures. Although articular cartilage is a highly functional type of connective tissue, it lacks blood supply, lymphatic vessels, and neural innervations and is characterized by a low metabolic turnover. Nutrients necessary for the mainly anaerobic metabolism only reach the cartilage tissue through the synovial fluid and subchondral bone via diffusion. The avascular environment causes the cartilage to have limited regenerative abilities (Fox et al., 2009, Chen et al., 2017b, Glaser and Putz, 2002, Bhosale and Richardson, 2008, Villalvilla et al., 2013, Akkiraju and Nohe, 2015). Because of that, degenerative changes are likely

to occur in such tissue, as at one point, the cartilage degradation exceeds its regenerative capabilities.

Articular cartilage is primarily made up of the extracellular matrix (ECM). ECM is mainly composed of collagen type II (Akkiraju and Nohe, 2015, Guilak et al., 1999, Lahm et al., 2010, Poole et al., 2002), water, and proteoglycans (PGs) which contain glycosaminoglycans (GAGs) (Ng et al., 2017). Components present to a smaller extent include several types of glycoproteins and non-collagenous proteins, for example, fibronectin and laminin (Gao et al., 2014). Type II collagen creates the cartilage framework to provide stability and extensibility. The hydrophilic properties of PGs permit water preservation within the ECM, which accounts for the mechanical and tensile strength of the articular cartilage (Ng et al., 2017).

Dispersed throughout the ECM are chondrocytes, the sole cartilage cell type. They synthesize ECM components and they are necessary for homeostatic regulation of the articular cartilage. The articular cartilage is separated into the superficial, middle, and deep zone (Chen et al., 2001, Antons et al., 2018). Depending on the zone, chondrocytes vary in size, shape, and number (Fox et al., 2009). Chondrocytes of the superficial and middle zone mainly synthesize collagen type II, IX, XI, and proteoglycans. The predominant collagen type II makes up 90-95% of the total collagen in the ECM and forms fibers and fibrils interwoven with PGs, for example, aggrecans. Collagen type IX and XI only account for 5-10% of the total collagen. They are essential for collagen fibril integration in the ECM. In the deep zone, chondrocytes mainly synthesize collagen type X (Akkiraju and Nohe, 2015), a nonfibrillar, network-forming collagen type (Debiais-Thibaud et al., 2019). The stiffness of the articular cartilage depends on the depth of the cartilage zone, collagen orientation, and extent of cartilage degeneration (Kempson et al., 1968). Previous research has described an increase in cartilage stiffness from the superficial to the deep zone (Antons et al., 2018, Chen et al., 2001).

The major component of articular cartilage, considering its wet weight, is water, which makes up approximately 80% of the superficial zone. The water

concentration decreases to 65% in the deep zone. It is most abundant in the pore spaces of the matrix, which is the intrafibrillar space within the collagen. The intracellular space only contains a minor amount of water. Water movement through the cartilage allows the passive transport and distribution of nutrients to the chondrocytes and provides joint lubrication (Fox et al., 2009). The compressive stiffness of articular cartilage is positively related to GAG concentration and negatively related to tissue hydration. When articular cartilage is compressed, proteoglycans and interstitial fluid interactions provide stress resistance at a high dynamic loading rate (Laasanen et al., 2003, Li et al., 2021).

1.2.2. Microenvironment of the chondrocyte

Articular cartilage is almost entirely composed of ECM. The remainder consists of chondrocytes scattered throughout the ECM. (Fox et al., 2009). They are directly surrounded by an approximately 2-4 µm thick layer of specialized ECM, the pericellular matrix (PCM), also referred to as the microenvironment of the chondrocyte. With a unique composition, the PCM predominantly contains type VI collagen and perlecan (Xu et al., 2016, Guilak et al., 2018). Other components include laminins, nidogens, hyaluronan, and biglycan (Sun et al., 2017, Zhao et al., 2020), which all contribute to the structural and biomechanical characteristics of the PCM. As the PCM separates the chondrocyte from the surrounding ECM, it establishes the communication between the chondrocyte and the ECM, which speaks for the essential role of the PCM in chondrocyte homeostasis. Collagen fibrils of the PCM retain the chondrocyte width and volume when compression forces are exerted onto the tissue (Wilusz et al., 2012, Zhang, 2015). Such characteristics could explain why OA-related PCM destruction impairs the biomechanical function of the cartilage and consequently decreases resistance to compressive forces.

The chondrocyte is fixed to the PCM by collagen type VI, which is attached to beta-integrin receptors and transmembrane proteoglycan NG2 of the chondrocyte membrane. The collagen fiber shell of the PCM enables it to alter the deformation behavior of chondrocytes, which is vital for the metabolic activity

of the chondrocyte (Julkunen et al., 2009, Han et al., 2007). In the case of a lowered amount of collagen type VI in the PCM, which is believed to be present in osteoarthritic cartilage, the mechanical properties of the PCM deteriorate (Zelenski et al., 2015, Danalache et al., 2019b).

As mentioned above, the articular cartilage of the knee joint can be divided into several zones. This separation exists as each zone comprises a unique cellular phenotype and ECM and PCM composition (Ge et al., 2006, Gao et al., 2014, Antons et al., 2018, Chen et al., 2001). In the superficial zone, chondrocytes are flat, elongated, and mainly appear as strings, while collagen fibers run parallel to the surface and are densely packed to protect the underlying zones. In the middle zone, chondrocytes appear more spherical, and collagen fibers run diagonally. Spherical appearing chondrocytes also appear in the deep zone with collagen fibrils positioned perpendicular to the surface. Chondrocytes of the middle and deep zones appear as single or multiple chondrocyte columns (Ng et al., 2017, Rolauffs et al., 2008).

The chondrocyte density is the highest in the superficial zone and decreases towards the deep zone, i.e., the relative proportion of chondrocyte to ECM decreases towards the deeper zones (Schumacher et al., 2002). Mechanical properties between the PCM and ECM also differ throughout the zones, although the PCM continuously shows a lower stiffness than its adjacent ECM (Darling et al., 2010). PCM stiffness differences between the cartilage zones seem to only exist to a minor extent. However, the ECM shows a relatively lower stiffness in superficial cartilage zones than in the deeper zone. Hence, in deeper zones, the ECM stiffness is relatively higher; therefore, the difference in the stiffness of ECM and PCM is also increased. The stiffness difference between the ECM and PCM in the deeper zones contributes to stress amplification and depicts the PCM as a transmitter of biomechanical signals (Wilusz et al., 2014, Alexopoulos et al., 2003). These properties of the PCM suggest that the PCM functions in providing a uniform cellular strain environment for the chondrocyte as ECM biomechanical properties vary with zonal localization. A loss of the PCM mechanotransduction function may impact the homeostasis of the chondrocyte negatively, which

contributes to the development or progression of OA (Zhao et al., 2020, Masutani et al., 2020).

Lower diffusivity of the PCM, compared to the ECM, implies that the PCM acts as a barrier for chondrocytes, as it controls the molecular exchange between the chondrocyte and the surrounding ECM. All substances synthesized by the chondrocyte first pass through the PCM before entering the ECM. Such a regulation mechanism suggests that the PCM plays a crucial role in matrix macromolecule synthesis and function (Leddy et al., 2008). The mentioned regulatory functions of the PCM may be interrupted by aging or disease such as OA (Zelenski et al., 2015).

1.3. Osteoarthritis

1.3.1. Epidemiology and diagnosis

OA is among the top causes of disability worldwide (Neogi, 2013). The 2014/2015 GEDA-study (Gesundheit in Deutschland aktuell) by the Robert Koch-Institut showed that for adults above 18 years, the OA prevalence for women was 22% and 14% for men. This number increases drastically in adults over 65 years, with an OA prevalence of 48% for women and 31% for men (Fuchs et al., 2017). The prevalence is expected to increase further due to the increasing rates of aged and obese people within the population (Hunter and Felson, 2006, Zhang et al., 2020). Besides age, other risk factors for OA include female sex (Arya and Jain, 2013), hereditary predisposition, obesity, diabetes, hypertension (Zheng and Chen, 2015, Eymard et al., 2015), macrotrauma, and continual microtrauma (Hassanali and Oyoo, 2011, Michael et al., 2010), which all contribute to the high prevalence of OA.

OA is primarily a clinical diagnosis based on physical examination and the history of the patient (Sinusas, 2012, Hunter and Felson, 2006), whereas radiography is used to support the diagnosis. Radiography is the most popular imaging diagnostic for OA. It enables visualization of osteophytes, bone cysts,

subchondral sclerosis, and narrowing of the joint space, which are typical indications of OA (Tanamas et al., 2010).

1.3.2. Therapeutic strategies

OA therapy aims to reduce pain and joint stiffness, to maintain or improve joint function, and to prevent or delay OA progression. Conservative treatment strategies are non-pharmacological or pharmacological. Lifestyle changes, including specific diet programs and moderate exercise, improve physical function and decrease joint pain (Arya and Jain, 2013). Orthotics, which aim to reduce contact forces within the joint, are also used as a symptomatic treatment. Pharmacological treatment includes nonsteroidal anti-inflammatory drugs (NSAIDs) and opioids.

Regarding surgical intervention, autologous chondrocyte implantation (ACI) has proven to be the most notable tissue engineering therapy. In ACI, ex vivo grown chondrocytes harvested from the patient in a first arthroscopic surgical procedure are implanted in a second-step surgery to repair cartilage defects. Other popular surgical interventions are high tibial osteotomy to alter the load-bearing axis of the leg, arthroscopic debridement, microfracturing, osteochondral cylinder transplantation, and total knee replacement (Arya and Jain, 2013, Katz et al., 2010).

The symptom severity, OA stage, and other individual factors such as age and comorbidity of the patient are the basis for the treatment choice (Rönn et al., 2011). In early OA stages, conservative treatment is applied, which alleviates OA symptoms but does not seem to have a notable effect on OA progression. If non-surgical therapy proves unsuccessful and the patient is still unable to perform regular daily activities, a total knee replacement should be considered. Nevertheless, after surgery, the patient is encouraged to exclude running or sprinting activities (Akkawi et al., 2015, Rönn et al., 2011), demonstrating that despite surgical therapy, the quality of life of the patient is still diminished.

The current OA research investigates the underlying mechanisms of the disease to develop therapeutic approaches that inhibit the progression of degenerative processes or to even allow osteoarthritic changes to be reversed. The early detection of OA-related changes is a prerequisite for developing and implementing effective prevention and treatment strategies (Imer et al., 2009b). However, as the pathological mechanisms of OA are only poorly understood, early diagnostic and therapeutic strategies are yet limited (Chen et al., 2017a).

1.3.3. Pathogenesis and pathophysiology

On a cellular level, OA results from chondrocyte incapacity to regulate the turnover of ECM components, which is mainly collagen type II (Man and Mologhianu, 2014, Akkiraju and Nohe, 2015). The reduction of intact collagen type II impairs the integrity of the cartilage collagen network, which leads to the formation of cartilage splits, known as fibrillations. In order to compensate for the loss of collagen type II, chondrocytes appear to increase the synthesis of collagen type I. In a healthy state, collagen type I is mainly present in subchondral bone tissue and is typically almost entirely absent in articular cartilage (Maldonado and Nam, 2013, Lahm et al., 2010, Roberts et al., 2009). The cartilage damage observable in earlier OA stages manifests at the articular surface as fibrillations, which initially run parallel to the surface. As the degeneration progresses, fibrillations orientate perpendicular to the surface and ultimately involve the subchondral bone. This degenerative process may take 20-30 years to occur but develops more rapidly in cases of cartilage trauma (Poole et al., 2006).

The precise pathophysiology of OA, especially that of the early disease stages, is unknown; however, it is believed that OA is caused by chondrocyte-mediated inflammatory responses (Konttinen et al., 2012). OA-related inflammation is characterized by increased activity of local proteolytic enzymes, which induce the formation of proinflammatory wear particles, which essentially are cartilage breakdown products. At one point in the course of OA, the formation of wear particles surpasses the ability of the immune system to eliminate them, and they accumulate within the synovial fluid. Wear particles further promote joint

inflammation and stimulate chondrocytes to release degradative enzymes, contributing to cartilage degeneration (Man and Mologhianu, 2014, Revell, 2008, Roach and Tilley, 2007).

As proteolytic degradation products, including wear particles, are released into the synovial fluid, they cause synovitis, a central element of osteoarthritic cartilage degeneration. Consequently, the synovial membrane synthesizes further proinflammatory cytokines, which mainly mediate the catabolic processes present in articular cartilage during OA. They subsequently stimulate chondrocytes to produce further proinflammatory cytokines, including tumor necrosis factor (TNF)-a, interleukin (IL)-1ß, IL-6, IL-15, IL-17, IL-18, leukemia inhibitory factor (LIF) (Wojdasiewicz et al., 2014, Mabey and Honsawek, 2015, Raman et al., 2018). These further exert catabolic functions, damaging and degrading cartilage (Hassanali and Oyoo, 2011).

Inflammatory mediators, as well as mechanical stress, induce NF-κB pathways, which mediate chondrocyte activation and induce the expression of matrix metalloproteinases (MMPs), disintegrin, and metalloproteinase with thrombospondin motifs (ADAMTSs) (Choi et al., 2019). As groups of proteolytic enzymes, they mediate catabolic processes in articular cartilage, such as collagen type II and aggrecan degradation (Goldring and Otero, 2011, Yang et al., 2017). Moreover, evidence suggests that the complement system and synovial macrophages contribute to the pathogenesis of OA, where they become chronically activated, trigger cytotoxic effects, and stimulate inflammation (Orlowsky and Kraus, 2015, Struglics et al., 2016).

Proinflammatory mediators and proteolytic enzymes (MMPs, ADAMTSs) are responsible for a vicious cycle of ECM degradation, a key characteristic of osteoarthritic cartilage degeneration (Goldring and Goldring, 2004, Rustenburg et al., 2018). Degenerative processes include biomechanical and biochemical changes such as changes in chondrocyte spatial organization and the increased release of degrading and proinflammatory enzymes and cytokines, which altogether play a role in the onset and progression of OA. (Man and Mologhianu, 2014, Maldonado and Nam, 2013, Lahm et al., 2010).

1.3.4. OA classification approaches and limitations

At present a universally adopted classification of healthy and osteoarthritic cartilage does not exist because of a lack of a standardized OA biomarker. The most common OA classification system is a clinical system, the International Cartilage Repair Society (ICRS) cartilage injury classification. It classifies the stages of OA macroscopically and it is based on the quantity and depth of cartilage lesions, visualized by arthroscopy, and may additionally include magnetic resonance imaging (MRI) (Harris and Flanigan, 2011). However, the earliest OA-related cartilage changes might not be detectable macroscopically or through MRI, potentially limiting the ICRS cartilage injury classification.

The Kellgren-Lawrence system, which is based on radiological assessment, is another widely used OA classification system (Kohn et al., 2016). A limitation of such a classification is that with radiography, one cannot directly assess articular cartilage, as radiography only provides two-dimensional images of three-dimensional calcified structures. Radiography does not allow a sensitive measure of early OA changes as radiographic changes are only detected with significant disease present. Considering these limitations, radiographs appear incapable of differentiating early osteoarthritic cartilage degeneration stages from intact cartilage (Attur et al., 2013, Wang et al., 2012, Stolz et al., 2009), which would be a desirable aspect of an OA classification method.

Other common OA grading systems include the Collins system, which macroscopically focuses on lesion size, bony changes, or cartilage surface configuration (Wilusz et al., 2013, Pritzker et al., 2006). The Mankin score (Histological Histochemical Grading System) consists of a microscopical evaluation of architectural, cellular changes, and histochemical staining. However, the validity of these grading methods in early OA stages has been questioned as both systems were only based on late-stage OA investigations (Pritzker et al., 2006, Ostergaard et al., 1999, Ostergaard et al., 1997). Furthermore, histological preparation itself causes destructive changes in the cartilage, limiting the validity of histochemical staining methods as OA grading systems.

Prognostic biomarkers found in blood, synovial fluid, or urine may act as markers of collagen breakdown and synthesis (Attur et al., 2013) representing OA cartilage degeneration. However, a limitation is that such biomarkers are not joint-specific, and they cannot be differentiated from biomarkers of physiological cartilage turnover. Additionally, distinctive features between normal age-related processes and osteoarthritic biomarkers are limited, hindering their differentiation (Lotz et al., 2014). Lastly, such prognostic biomarkers may correlate with the presence of OA and the extent of the disease; however, they do not directly present information about the local topographical cartilage deformation present at the affected joint, limiting their practical applicability.

1.3.5. Chondrocyte spatial organization

A refined, microscopic approach for the direct classification of healthy cartilage and stages of osteoarthritic cartilage has been established by Felka et al., which focuses on the spatial organization of chondrocytes. It has been described that as OA initiates and progresses, chondrocytes alter their spatial arrangement into different patterns. These observable alterations of the spatial chondrocyte organization include single strings (SS), double strings (DS), small clusters (SC), big clusters (BC), and eventually a diffuse chondrocyte arrangement, which sequentially arise, depending on the severity of local OA-related degenerative changes (Figure 1) (Felka et al., 2016, Danalache et al., 2019b, Danalache et al., 2021).

In healthy and intact cartilage areas of the femoral condyles, chondrocytes are predominantly present as singular lines, known as single strings. However, with the onset of OA, chondrocytes can increasingly be found as double string arrangements, where chondrocytes are aligned parallelly in two lines. In the late stages of OA, chondrocytes appear as circular aggregations known as small clusters or big clusters, depending on the number of chondrocytes found in the aggregation (Rolauffs et al., 2010, Felka et al., 2016, Danalache et al., 2019b).

The precise mechanism of the occurrence of spatial chondrocyte organization is still unclear. It has been suggested that spatial organization changes occur by cellular proliferation (Aicher and Rolauffs, 2014). However, as mitotic figures appear to be absent in chondrocytes of osteoarthritic cartilage, it is possible that chondrocyte aggregation into clusters occurs by active cell migration rather than by cellular proliferation (Kouri et al., 1996). The spatial remodeling processes of chondrocytes have been proposed to act as an image-based diagnostic marker to detect OA preclinically. Spatial chondrocyte organization can be easily determined using already clinically available technology through confocal endomicroscopy (Tschaikowsky et al., 2021). However, further investigations are necessary for a potential application and integration of the image-based marker into the clinical setting (Aicher and Rolauffs, 2014, Felka et al., 2016, Rolauffs et al., 2011, Tschaikowsky et al., 2021).

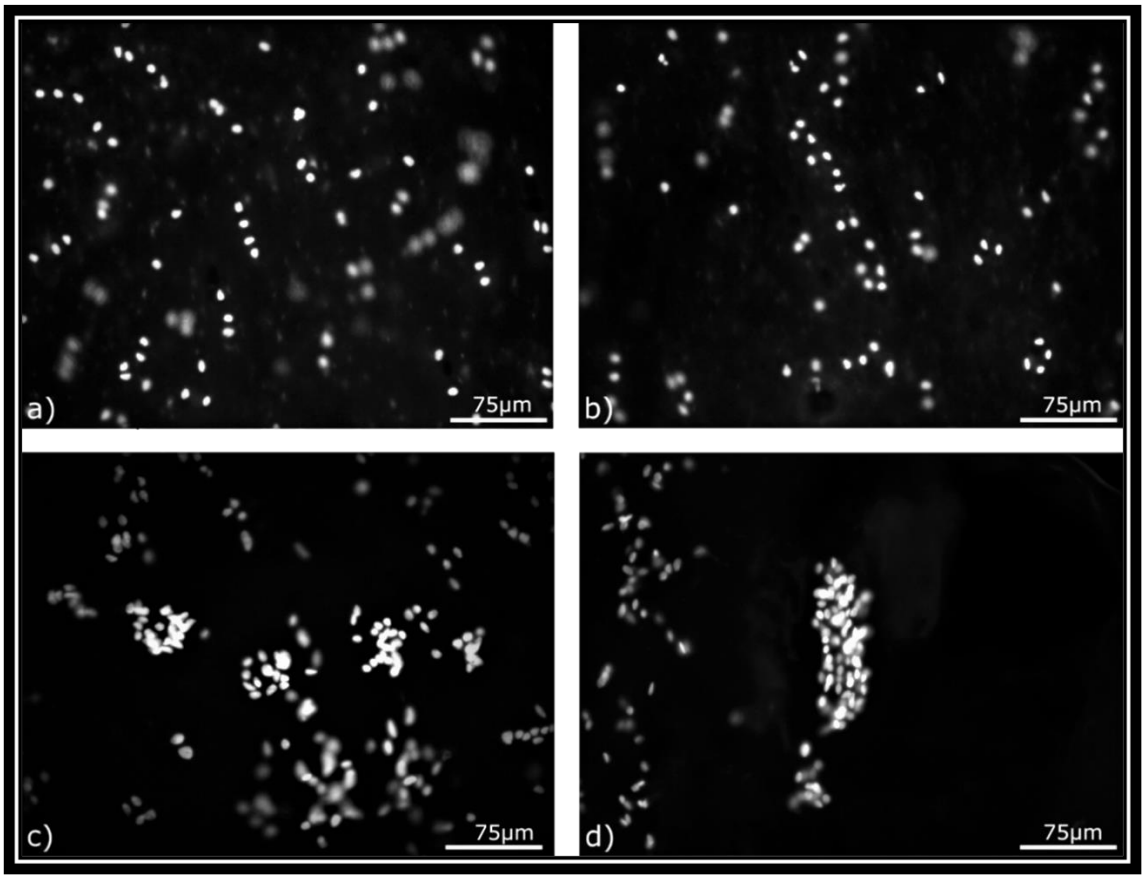

Figure 1. Alteration of the spatial organization of knee joint chondrocytes during the onset and progression of OA. *Pictures* ***a)-d)*** *show the microscopic images of DAPI nuclear staining of chondrocytes (depicted in white). Change in the spatial chondrocyte organization is observed as OA progresses.* ***a)*** *Single strings can be observed in healthy cartilage areas.* ***b)*** *At the onset of OA, double strings appear increasingly.* ***c)*** *As the degeneration proceeds, small clusters arise,* ***d)*** *followed by big clusters.*

1.4. AFM application for the investigation of OA

1.4.1. AFM basics

Atomic force microscopy (AFM) has widely been represented as a suitable approach for the investigation of elastic properties and topography of the cartilage surface (Desrochers et al., 2010, Imer et al., 2009b, Park et al., 2004, Park et al., 2009, Tomkoria et al., 2007). This high-resolution measurement technique enables the analysis of the disintegration of the cartilage macromolecular network present in OA (Desrochers et al., 2010) and, therefore, facilitates the detection of early osteoarthritic changes.

AFM possesses the ability to assess biological samples at the nanoscale. This quality is a crucial advantage of AFM compared to other OA investigation techniques, as early OA stages appear to be first detected on a nanoscale (Stylianou et al., 2019, Stolz et al., 2009). Another benefit of the technique is that it analyzes structural and biomechanical changes directly at the surface of osteoarthritic cartilage, where OA-related changes first appear (Poole et al., 2006, Desrochers et al., 2010).

Apart from AFM, the micropipette aspiration technique represents an efficient method to investigate the biomechanical properties of chondrocytes (Wang et al., 2007). In this technique, the mechanical deformation of a single chondrocyte and its surrounding PCM is measured in response to a predefined aspiration pressure applied by a micropipette (Jones et al., 1999). A major limitation of the technique is, however, that it does not allow the investigation of the ECM, which makes up the largest proportion of the articular cartilage and should therefore not be excluded when analyzing biomechanical properties of articular cartilage (Fox et al., 2009). For this reason, AFM presented itself as a more suitable approach for the present study as it permits the investigation of all parts of the articular cartilage matrix.

AFM operates with a 1-5 mm long microfabricated AFM probe made from silicon or silicon nitride with a metallic coating usually consisting of aluminum or gold. The main component of the standard AFM probe is the cantilever chip, which features different cantilevers. The featured cantilevers are several nanometers in size and are located at the side edges of the cantilever chip (Sumbul et al., 2018). At the outer end of the cantilever, the cantilever tip is located, which is the unit of the AFM probe that is in direct contact with the sample. Optionally a polystyrene microsphere can be attached to the cantilever tip, which acts as a connecting element between the cantilever tip and the sample surface.

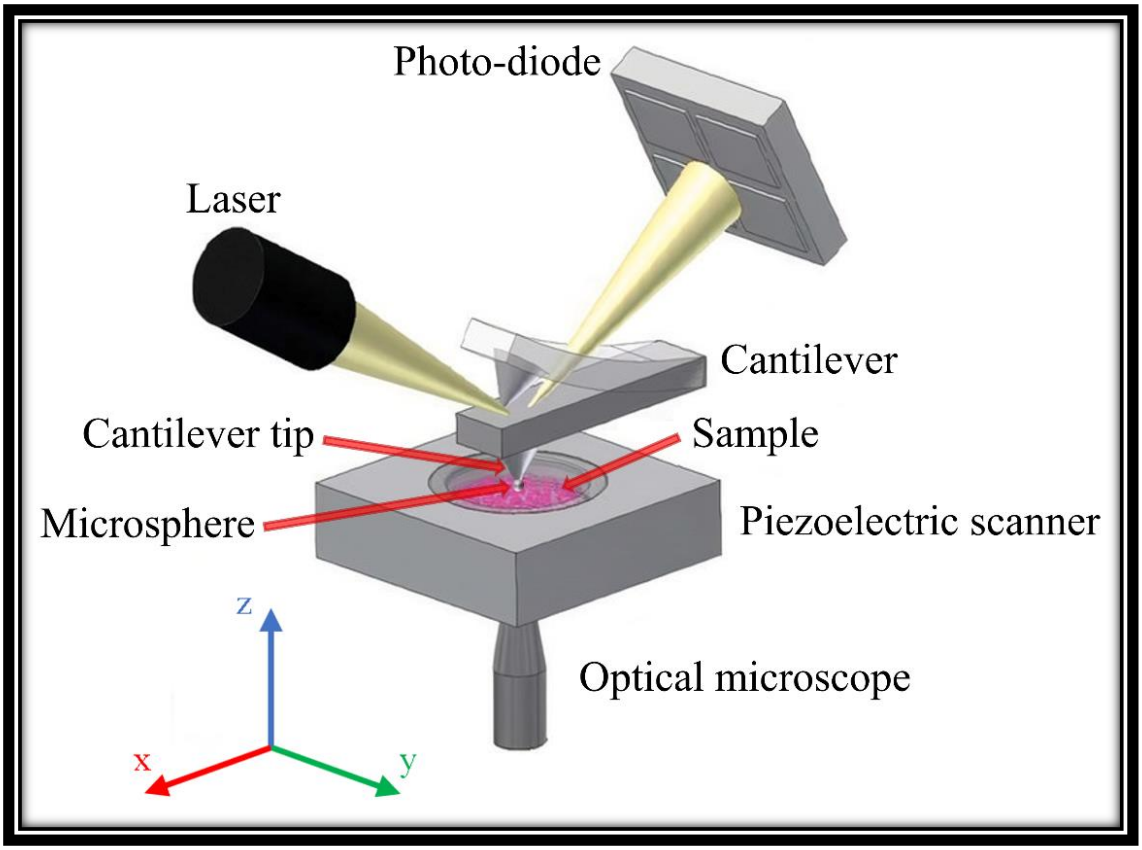

Figure 2. Schematic diagram of the AFM setup. *The biological sample is microscopically observed with an inverted optical microscope integrated into the AFM unit. Connected to the AFM probe is the cantilever, which interacts with the sample surface. Attached to the tip of the cantilever is a microsphere. The piezoelectric scanner provides the accurate movement of the sample in all three axes (x-y-z-), which allows precise positioning of the cantilever at specific regions or even at single cells of the biological sample, allowing their investigation. Displacement of the cantilever is measured with the optical lever method. A laser beam, which is reflected by the upper surface of the cantilever, is detected by the four-segment photo-diode. The illustration was obtained from (Danalache, 2020) and is used with the kind approval of Marina Danalache.*

The AFM probes and their featured cantilevers are available with different mechanical characteristics and geometrics, each with unique functional properties. When the AFM probe is in close proximity to the sample surface, the cantilever senses generated interaction forces between the sample surface and the AFM probe, mainly van der Waals forces, electrostatic forces, and electronic repulsions (Roa et al., 2011).

The AFM piezoelectric scanner, a navigable unit of the AFM controlled by micro-positioners, moves the sample on the x-y-z-axis. This manoeuvering allows accurate positioning of the cantilever onto the area of interest of the sample.

Displacement or bending of the cantilever is measured with a laser beam focused on the upper surface of the cantilever and reflected onto a four-segment photo-diode. The photo-diode detects and processes the reflected laser signal. With a set of mirrors, the laser beam can be adjusted appropriately. As the cantilever tip or microsphere contacts the sample and indents into it, surface properties and interaction forces cause displacement of the cantilever. The displacement is detected as deflections of the laser beam occur, measured by the photo-diode (Danalache, 2020). Thus, as the cantilever scans the sample surface, the photo-diode detects deflection on the horizontal plane (x-y-axis) and vertical plane (z-axis) (Figure 2).

Deflections detected on the vertical plane (z-axis) are necessary to calculate the distance between the AFM probe and the sample surface, as well as the indentation depth of the cantilever tip or microsphere into the sample surface (Brückner et al., 2017, Imer et al., 2009a). For these calculations, the generation of force-distance curves is necessary.

1.4.2. AFM force-distance curve

Force-distance curves are generated by AFM measurements and allow photo-diode detection data (photodetector voltages and z-piezo positions) to be converted into the unit of force (Nanonewtons) and into AFM probe-sample distance (Nanometer) (Eppell et al., 2016). This conversion is necessary for the AFM to calculate the Young's modulus (YM), a mechanical property used to describe the stiffness of a material surface quantitatively. To generate a force-distance curve, the cantilever tip first approaches the surface and subsequently contacts it until a predefined force (305.144 nN) is exerted on the surface (Figure 3). The approach of the cantilever is also referred to as the loading phase. The cantilever tip retracts when the predefined force is reached, also termed the unloading phase (Imer et al., 2009a).

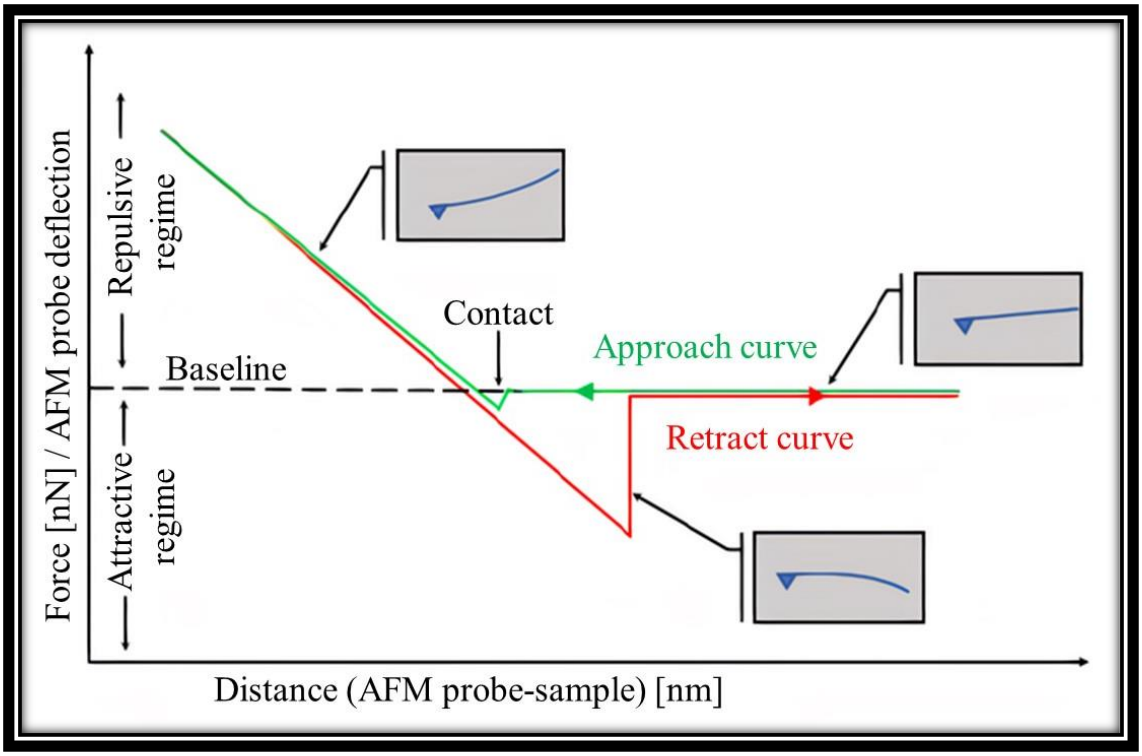

Figure 3. Schematic force-distance curve depicting the cantilever interaction with the sample surface. *The interaction cycle consists of three phases: approach (green line), contact, and retraction (red line). The x-axis describes the distance (nm) between the cantilever tip of the AFM probe and the sample surface and the subsequent indentation depth. The AFM probe-sample distance is determined by the z-piezo position, which is registered by the photo-diode. The y-axis refers to the force (nN) exerted onto the sample surface and, respectively, the AFM probe deflection detected by the photo-diode. The illustration was obtained from (Danalache, 2020) and is used with the kind approval of Marina Danalache.*

As the cantilever tip approaches the sample surface, the AFM probe-sample distance decreases as the z-piezo position alters. In the loading phase, the force applied to the sample or the vertical deflection of the probe, detected by the photo-diode, remains unchanged. At a given distance from the sample surface, attractive forces impact the cantilever tip, which causes it to snap onto the surface. As the cantilever tip indents into the tissue, the force applied to the surface increases continuously until the predefined force setpoint (305.144 nN) is reached. The resulting displacement of the cantilever causes a deflection change of the laser beam on the upper surface of the cantilever, detected by the photo-diode. In the subsequent retraction, attractive forces play a more prominent role than during the cantilever approach. Due to adhesion forces, negative deflections of the cantilever can be detected as the cantilever tip remains in

contact with the sample surface until the adhesion forces are overcome (Danalache, 2020, Imer et al., 2009a).

During the loading phase, as the AFM probe-sample distance decreases and the cantilever tip indents into a sample surface with high stiffness, the force setpoint is reached earlier in the interaction cycle than in a material with lower stiffness because the surface with higher stiffness deforms less. Thereby the force-distance curve reflects on the individual elastic properties of a sample surface. Viscoelastic properties (i.e., stiffness) are investigated as the cantilever comes in contact with the surface and exerts a defined force onto it. In such a way, the generation of a force-distance curve allows the AFM to calculate the YM to determine the stiffness of a material surface (Danalache, 2020, JPK Instruments AG, 2021b).

1.4.3. Cartilage stiffness investigation with the Young's modulus

The YM is a mechanical property that characterizes the stiffness of solid materials and it describes the elastic deformation of a material under mechanical loading. The AFM determines the YM by processing force-distance curves of sample surface measurements and thereby allows a quantitative assessment of the surface stiffness of a material (Vinckier and Semenza, 1998). The YM (E), expressed in Pascals, is defined as the ratio of tensile stress to tensile strain. Whereas tensile stress (σ) is defined as the force (Newton) per unit area ($\frac{\mathrm{F}}{\mathrm{A}}$) and tensile strain (ε) is the ratio of change in length (Nanometer) to the initial length ($\frac{\Delta l}{lo}$) (Chen, 2016).

Equation 1. $$E = \frac{tensile\ stress}{tensile\ strain} = \frac{\sigma}{\varepsilon}$$

Equation 1.1. $$\sigma = \frac{force}{area} = \frac{F}{A}$$

Equation 1.2. $$\varepsilon = \frac{deformed\ length - initial\ length}{initial\ length} = \frac{li - lo}{lo} = \frac{\Delta l}{lo}$$

The tensile stress (N) is a configurable and predefined parameter of the AFM, which describes the force that the AFM probe, or rather the cantilever tip with its attached microsphere, exerts onto the sample surface area. In terms of the AFM, the tensile strain can be viewed as the indentation depth (nm) of the microsphere into the sample surface. Here ε is calculated by subtracting the length of the cantilever deflection (x) from distance z, which is the distance the cantilever travels in the direction of the sample, from the point where it touches the surface up to the point where the predefined force is reached (Figure 4) (JPK Instruments AG, 2021a). At this point, the cantilever retraction occurs (Figure 3).

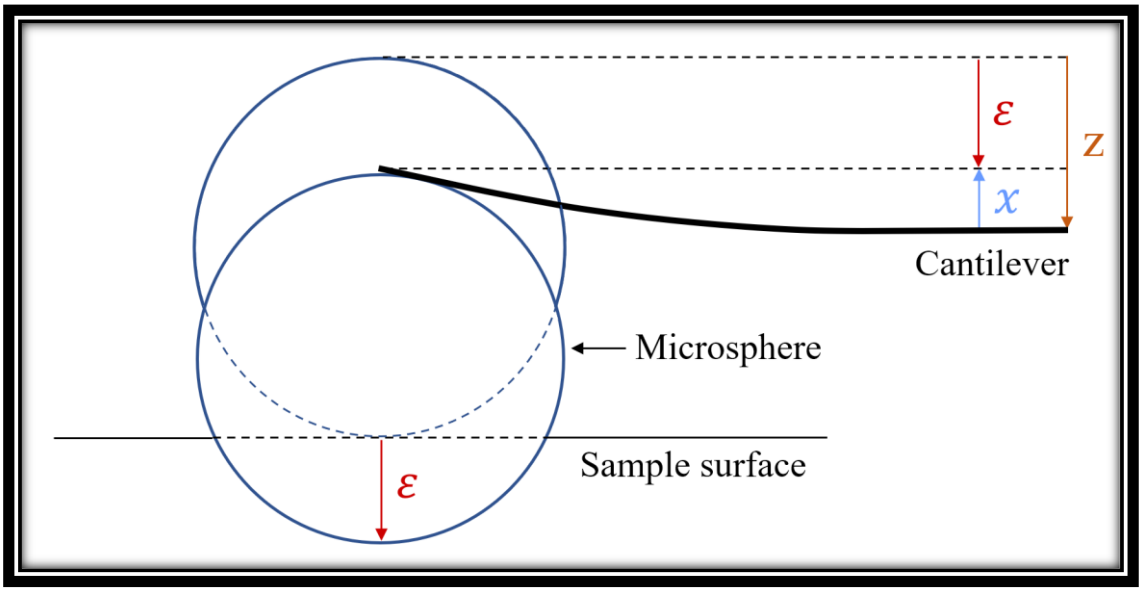

Figure 4. Schematic illustration of the microsphere indentation into the sample surface. *The cantilever covers a certain distance (z) in the direction of the sample, from the point where it touches the surface up to the point where a predefined force is reached. At this point, a specific cantilever deflection is present (distance x), which depends on the mechanical properties (i.e., stiffness) of the surface. For the calculation of the tensile strain (ε), distance x is subtracted from distance z.*

The higher the YM, the stiffer the sample surface and, thus, the higher its resistance to elastic deformation since the same force per unit area applied by the AFM causes a relatively smaller change in indentation depth than it does in a less stiff material (Chen, 2016). In other words, a material with a higher stiffness can sustain more external force with less deformation than a material with lower stiffness (Rivin, 2010).

1.5. Aim of the thesis

A better understanding of the underlying processes of OA is required to further improve treatment possibilities and develop diagnostic procedures to allow early OA detection. It has already been described that OA-related changes in spatial chondrocyte organization go hand in hand with a stiffness reduction of the PCM (Danalache et al., 2019b). In the present study, the stiffness of the ECM and PCM and their interrelationship are evaluated based on changes in the spatial chondrocyte organization as a marker for OA-related local tissue degeneration.

Studies where the ECM and PCM stiffness of healthy cartilage was examined with the micropipette aspiration method or AFM have suggested that the ECM possesses a significantly higher stiffness than the PCM (Darling et al., 2010, Guilak et al., 1999). It has also been suggested that as OA progresses in the knee joint cartilage, the ECM and PCM stiffness decreases continuously, reflecting on a reduction in the structural integrity of the matrices (Wilusz et al., 2013, Stolz et al., 2009). However, the detailed relationship of OA-related stiffness changes of the ECM compared to the PCM has not been investigated in detail yet, which is a central aim of the present study.

Earlier studies have moreover suggested that as OA proceeds, the prevailing type II collagen is progressively replaced by collagen type I, which alters the structural integrity of the collagen network and decreases the mechanical stability of the ECM. (Maldonado and Nam, 2013, Lahm et al., 2010, Poole et al., 2002). For this reason, OA-related changes are additionally investigated qualitatively by means of immunofluorescence labeling of the ECM components collagen type II and collagen type I. The immunofluorescence staining results are then compared to the YM values acquired by AFM.

2. Materials and methods

2.1. Materials and equipment used

Table 1. Technical devices used in the thesis

Description	Article number	Manufacturer
CellHesion®200 (Atomic Force Microscope)	3833000999	JPK Instruments, Germany
Zeiss AxioPhot Fluorescent Microscope	42378	Zeiss, Germany
Leica DM IL LED Microscope	208809	Leica, Germany
Binder ED 53 Incubator	CB 210#02-40-42-5	Binder, Germany
Melag Typ 80 Incubator	9785238	Melag, Germany
Laser Scanning microscope (Observer Z1 fluorescence)	2435000430	Zeiss, Germany
Leica cryotome type CM3050S	3567	Leica Biosystems, Germany
ThermoMixer® Comfort	5355BM257870	Eppendorf, Germany

Table 2. Materials used for cartilage preparation

Description	Article number	Manufacturer
6-well cell culture plates	657160	Greiner Bio-one, Hungary
Amphotericin	KAT P11-00	Thermo Fisher Scientific, Austria
Biocompatible glue	n.a.	JPK instruments, Germany
DAPI (4′,6-diamidino-2-phenylindole)	D1306	Thermo Fisher Scientific, USA
Disposable scalpel	02.001.30.021	Feather, Japan
DMEM (Dulbecco's modified Eagle's medium)	41966-029	Gibco Life Technologies, USA
Petri dishes 145x20mm	639102	Greiner Bio-one, Hungary
Penicillin/streptomycin	P4333	Sigma Aldrich, USA
Tissue culture dish 40	93040	Techno Plastic P, Switzerland
Tissue-Tek®O.C.T.™ Compound	4583	Sakura Finetek Europa B.V., Netherlands

Table 3. Materials used for AFM measurements

Description	Article number	Manufacturer
AFM glass block	3833000999	JPK Instruments, USA
All-in-One-Al-TL Cantilevers	AIOAl-TL-10	Budget Sensors, Bulgaria
Ethanol	ETO-5000-99-1	SAV-LIQUID Production GmbH, Germany
Leibovitz's L-15 Medium	11415064	Gibco Life Technologies, USA
M-bond-610 Adhesive	G3203	Micro-measurements, Germany
Microspheres 25 µm	07313-5	Polysciences, Polybead®, USA
µ–Dish 35 mm, high ESS (elastically supported surface) (28 kPa)	81191	ibidi®, Germany

Table 4. Materials used for immunofluorescence staining

Description	Article number	Manufacturer
BSA (Bovines serum albumin)	A1391.0050	AppliCHem GmbH, Germany
DAPI (4′,6-diamidino-2-phenylindole)	D1306	Thermo Fisher Scientific, USA
Primary antibody anti-collagen I	Ab90395	Abcam, UK
Primary antibody anti-collagen II	MA5-12789	Thermo Fisher Scientific, USA
Formaldehyde solution 30%	4235.2	Carl Roth, Germany
Hyaluronidase	CAS 37326-33-3	Sigma-Aldrich, USA
Dulbecco's PBS (Phosphate-buffered saline)	14190250	Gibco Life Technologies, USA
Secondary antibody Alexa Fluor 594 (Goat Anti-Mouse IgG H&L)	Ab150116	Abcam, UK
Triton X-100	T9284	Sigma-Aldrich, USA
Superfrost ® Glass slides	03-0060	R. Langenbrick, Germany
Coverslips	01-1818/x	R.Langenbrick, Germany
Fluorescent mounting medium	S3023	Agilent Dako, USA

2.2. Cartilage sample preparation

The Department of Orthopedic Surgery of the University Hospital Tübingen, Germany and the Winghofer Medicum clinic (Rottenburg, Germany) provided cartilage samples for the present study. The utilization of the cartilage samples of the patients was approved with preoperatively obtained informed consent of the patients. Approval by the ethical committee of the Medical Faculty of the University of Tübingen had been obtained before the onset of the research project (project number 674/2016BO2).

Articular cartilage samples were examined from 30 patients in total who were aged 50-83 years. Of these patients, 18 were female and 12 were male. For each patient, one cartilage sample was prepared and used for AFM measurement and consecutive immunofluorescence staining. Histograms (Figure 5) illustrate the age and sex distribution data. Samples were exclusively obtained from patients diagnosed with severe knee osteoarthritis and who underwent total knee arthroplasty.

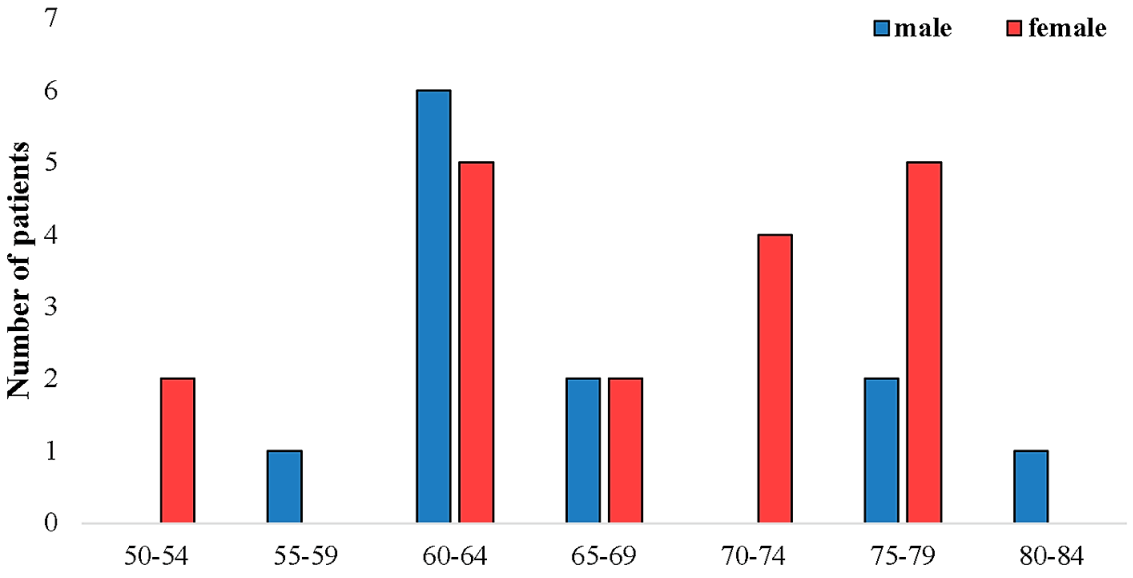

Figure 5. Histograms representing the age (in years) and sex distribution of the examined patients who underwent total knee arthroplasty. *In total 30 Patients were examined, 18 female (red) and 12 male (blue).*

During the arthroplasty, bone sections together with articular cartilage were removed from the femur and tibia in the knee joint region. The present study

obtained cartilage samples of interest from the distal femoral cut. Cartilage preparation and AFM measurements were conducted on the day of the operation or on the following day.

Articular cartilage of the medial and lateral femoral condyles was removed from the underlying subchondral bone with a scalpel and medical tweezers (Figure 6 a)). After surgical removal (Figure 6 b)), the cartilage was stored in collection cups that contained DMEM (Dulbecco's modified Eagle's medium), amphotericin B 1.2% (v/v), and penicillin/streptomycin 2% (v/v) to provide conservation of the removed cartilage and to prevent colonisation with bacteria or fungi.

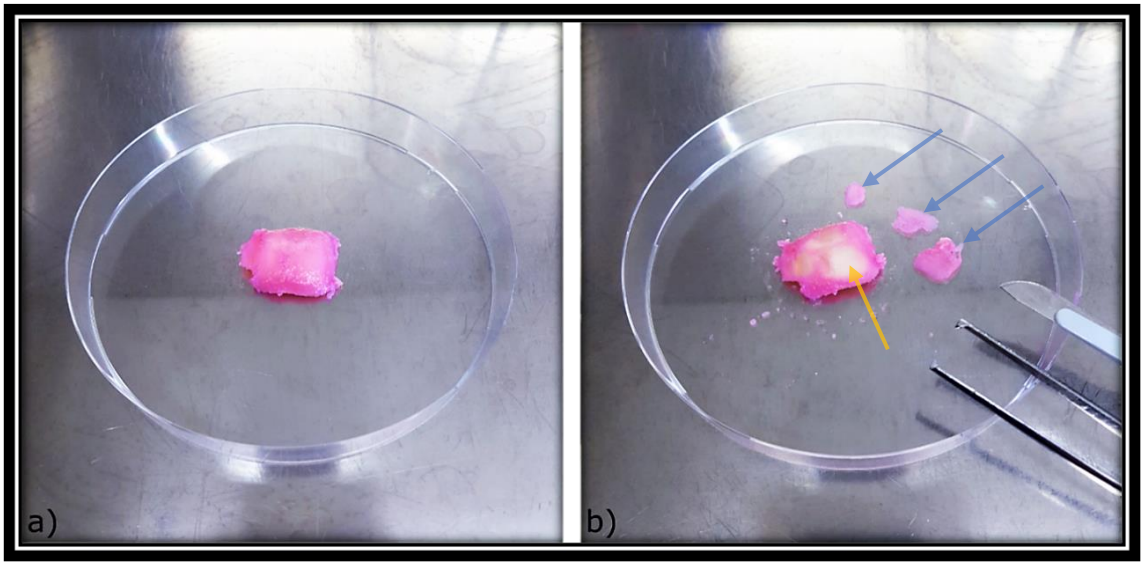

Figure 6. Illustration of a femoral condyle a) before and b) after cartilage removal from the subchondral bone of the examined patients who underwent total knee arthroplasty. *The blue arrows indicate removed cartilage, which was removed with a scalpel and medical tweezers. The orange arrow indicates the exposed subchondral bone after cartilage removal.*

Following this, the cartilage samples were embedded and frozen in Tissue-Tek® and subsequently sectioned into 35 µm thick sections using the Leica cryotome. The sections were washed with PBS (phosphate-buffered saline) and stained with DAPI (4′,6-diamidino-2-phenylindole) nuclear staining and they were then placed in 6-well cell culture plates. The sections were subsequently examined with the DMIRBE Leica Microscope to evaluate if all different spatial chondrocyte organizations (SS, DS, SC, BC) were present, which indicated that the section was suitable for AFM measurement immunofluorescence staining. One section

per patient was then fixated to a tissue culture dish 40 with biocompatible glue. Finally, Leibovitz's L-15 Medium was added to the tissue culture dish 40, covering the whole section to conserve the tissue. The prepared section was stored in the Belag incubator at 37°C until AFM measurements were performed.

2.3. AFM

2.3.1. AFM setup

The stiffness of the articular cartilage sections was investigated with AFM, which allowed the YM determination of the sample surface. Multipurpose AFM probes which contained four different tipless cantilevers were used. Cantilever tip C (Constant Force (k) = 7.4 N/m)) which measures 150 µm in size, was used in the present study. For the AFM setup, the AFM probe was first mounted onto the glass block (Figure 7 a)). Subsequently, the glass block was placed and fixed into the AFM head (Figure 7 b)). Following this, the AFM head was placed into a holder to position the glass block with the AFM probe directly above the AFM sample holder unit, which would later contain the tissue culture dish 40 with the cartilage sample.

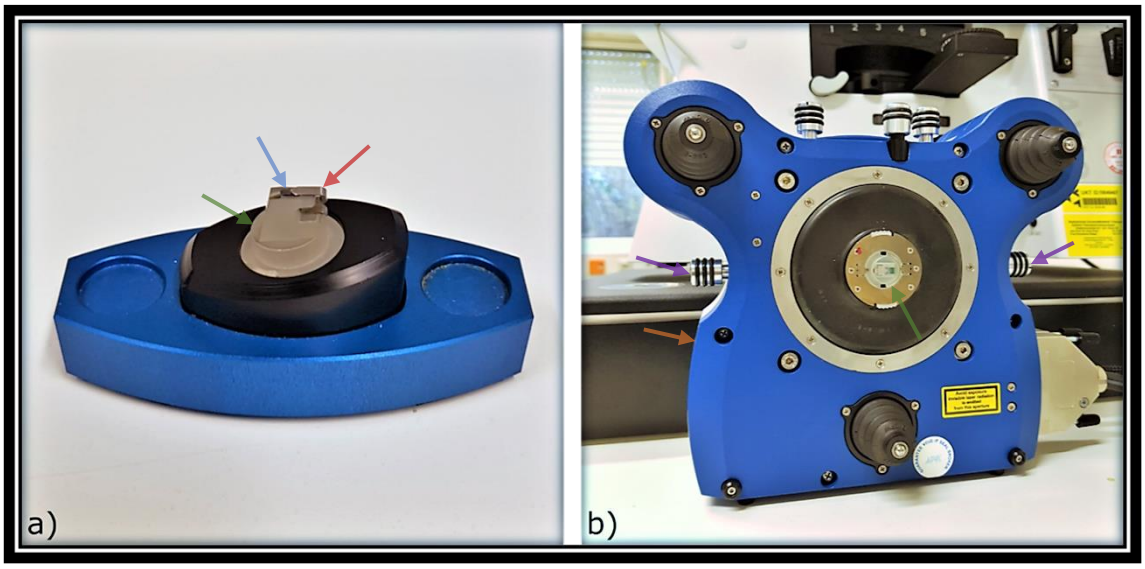

Figure 7. AFM setup: a) *The AFM probe (blue arrow) was mounted onto the glass block (green arrow) using a metal spring (red arrow).* ***b)*** *The glass block was then placed and fixed into the AFM head (orange arrow). Micro-positioners (purple arrows) were used to regulate piezoelectric scanner movement for cantilever positioning.*

Before operating with the AFM, a laser alignment was conducted. This process was necessary to assure maximum sensitivity of force appliance onto the measured sample and to allow accurate sample stiffness measurements. Cantilever displacement was detected by a laser beam that was prior focused on the upper surface of the cantilever. The reflected beam was detected by the center of a four-segment photo-diode (Figure 2). The total sum of all laser beams detected by the photo-diode is expressed in Voltage (V). The detected sum had to be > 1 V for maximal measurement sensitivity, as described by JPK Instruments AG. A sum > 1 V meant that a sufficient amount of laser beams were reflected by the cantilever surface and detected by the photo-diode. A detected sum value < 1 V had to be revised, as it demonstrates an AFM setup with insufficient laser beam detection by the photo-diode, yielding inaccurate and unreliable data (JPK Instruments AG, 2012).

2.3.2. Microsphere attachment to the cantilever tip

In the present study, polystyrene microspheres with a diameter of 25 µm were manually attached to the cantilever tip C for tissue stiffness measurements.

Microsphere attachment to the cantilever tip modifies the size and geometry of the indenting body and increases the interaction area between the cantilever tip and the sample surface. The microsphere attachment is optional and is conducted depending on the surface properties of the analyzed sample (Glaubitz et al., 2011). In the present study, microsphere attachment was conducted to reduce exerted pressure and indentation depth of the cantilever tip during YM measurements to obtain values averaged for the local tissue stiffness.

At first, the microspheres were placed in a 70% (v/v) ethanol solution in double-distilled water to establish a concentration of 1000 microspheres/µL. The M-bond-610 Adhesive was used to glue microspheres onto the cantilever tip. A glass slide was cleaned with a 70% (v/v) ethanol solution and wiped with a cellulose cloth so that the microsphere attachment onto the cantilever tip could occur on a clean surface. The glass slide was then placed on the AFM sample holder unit. The laser and mirror of the AFM were adjusted so that an approach could be conducted (i.e., Setpoint = 1.0 V), followed by a retraction, to position the cantilever exactly 100 µm above the glass slide.

The inverted optical microscope, which is integrated into the AFM, was removed so that approximately 1 µl of the diluted microsphere concentration could be placed on the glass slide center. The presence of microspheres in the dilution was verified using the inverted optical microscope. Approximately 1 µl of the M-bond-610 Adhesive was added alongside the dilution drop containing the microspheres. Ultimately, the cantilever was positioned above the adhesive with the guidance of micro-positioners that regulate the piezoelectric scanner movement. The cantilever was moved down onto the adhesive in 10 µm increments until the cantilever tip was fully immersed in adhesive. Cantilever contact with the adhesive was visualized by deflection changes of the laser, identified by the AFM photo-diode. Subsequently, the cantilever tip was retracted from the adhesive.

Following this, the cantilever was positioned directly above a microsphere. The attachment of the selected microsphere onto the cantilever tip was achieved with the following measurement parameters: Setpoint = 1.0 V, Pulling length = 90.0

µm, Section rate = 2000 Hz, Contact time = 120 sec. After successful attachment (Figure 8), the AFM head was removed. The glass block and the cantilever with its attached microsphere were placed in the Melag incubator at 60°C for 120 minutes. This final process was essential for drying the adhesive, allowing a stable attachment of the microsphere and the cantilever tip.

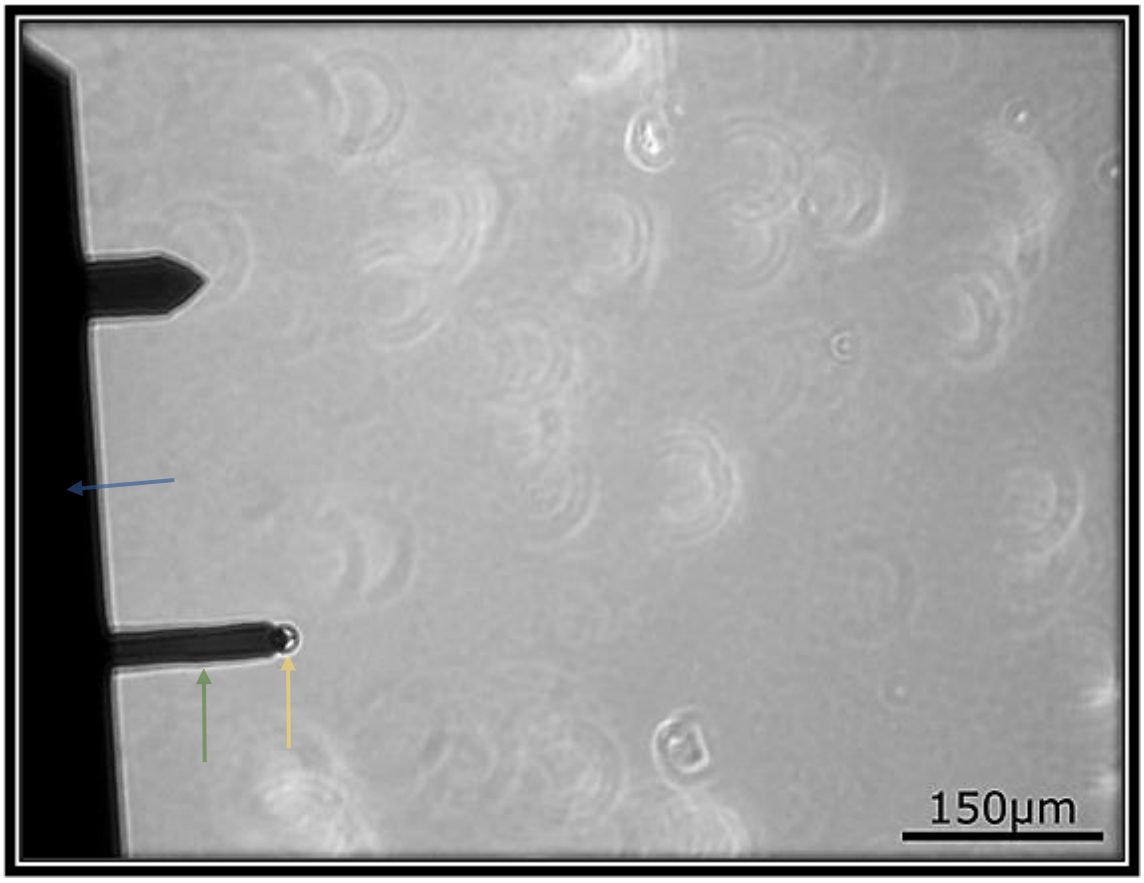

Figure 8. Cantilever-microsphere setup. *Illustration of a cantilever (tip C) with an attached microsphere (25 µm). The green arrow displays the cantilever (tip C), and the yellow arrow the successfully attached microsphere (25 µm) to the cantilever tip. The blue arrow indicates the side edge of the cantilever chip of the AFM probe.*

2.3.3. Cantilever calibration procedure

The cantilever was calibrated so that the vertical deflection would be expressed in units of force (Newton) instead of Volts (V), which it was before calibration. The first step of the calibration was to determine the sensitivity of the cantilever, allowing the vertical deflection to be expressed as a distance (nm). For the initial

step, a force-distance curve had to be obtained from a clean and firm surface; therefore, a measurement of a tissue culture dish 40 surface was conducted. The tissue culture dish 40 only contained Leibovitz's L-15 Medium to establish the same experimental environment, which would be present in later cartilage sample measurements. The following AFM measurement parameters were used for the calibration procedure: Setpoint = 1.0 V, Pulling length = 90.0 µm, Extended speed = 5 µm/s, Contact time = 0 sec., Z movement = Constant speed, Delay mode = Constant force, Section rate = 2000 Hz. The linear region of the acquired force-distance curve was selected to express the vertical deflection in nanometers (JPK Instruments AG, 2012).

Secondly, the spring constant of the cantilever was determined so that, ultimately, the cantilever deflection was displayed in Newtons (N). The spring constant determination was performed using a thermal noise method, which produced a noise spectrum. A fit range was selected from the first peak of the noise spectrum curve to display the vertical deflection in Newtons (JPK Instruments AG, 2012). The calibration process was repeated every time an AFM probe with a cantilever was mounted onto the glass block for AFM measurements. After calibration, the defined setpoint was 305.144 nN (Nanonewtons) and was adjusted to that value before each cartilage section measurement.

2.3.4. AFM measurement sensitivity

The calculation of a correction factor (Equation 2) was essential to verify and optimize the measurement sensitivity and validity of the cantilever tip and its attached microsphere. An individual correction factor was determined for each cantilever used in the present study. For the correction factor calculation, stiffness measurements were conducted on a reference sample surface with a predefined stiffness of 28kPa. The reference sample had prior been placed in a tissue culture dish 40. Before the measurement, the tissue culture dish 40 was filled with double-distilled water, with the entire reference sample submerged in water.

The number of measurements conducted at one location was presettable at the AFM. In the present study, nine consecutive AFM measurements were performed at three different positions on the reference sample. The median of the nine measurements per chosen position was calculated. Further, the different median values of the three different positions were used to calculate the arithmetic mean of all three positions, which yielded the mean reference sample stiffness (kPa). Lastly, the predefined stiffness value (28kPa) was divided by the mean reference sample stiffness (kPa) to determine the correction factor.

Equation 2. $$correction\ factor = \frac{28kPa}{mean\ referance\ sample\ stiffness\ (kPa)}$$

All obtained YM values of the ECM and PCM in the present study were multiplied with the corresponding correction factor of the used cantilever before further data processing to adjust the YM values considering the deviation from the predefined stiffness (28kPa) of the reference section (JPK Instruments AG, 2012).

2.3.5. Young's modulus measurement of articular cartilage

A 35 µm thick cartilage section was glued onto a tissue culture dish 40 with biocompatible glue. Subsequently, Leibovitz's L-15 Medium was added for tissue conservation. With the inverted optical microscope integrated into the AFM, visualization of the articular cartilage at a cellular level was possible. The phase-contrast microscope allowed the identification of the spatial chondrocyte organizations of interest, including single strings, double strings, small clusters, and big clusters (Figure 9).

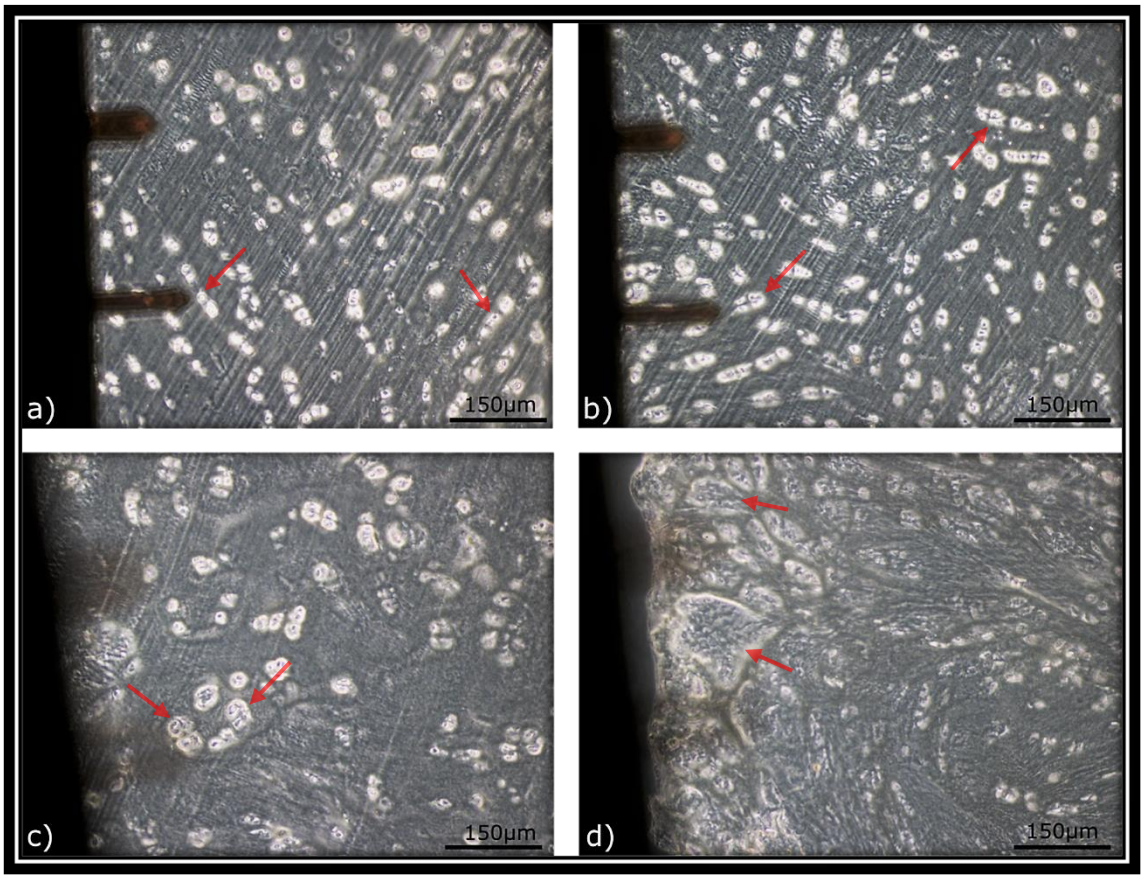

Figure 9. Microscopic visualization of a 35 µm thick cartilage section displaying spatial chondrocyte patterns in different stages of OA degeneration. *The red arrows indicate* ***a)*** *single strings,* ***b)*** *double strings,* ***c)*** *small clusters, and* ***d)*** *big clusters. Picture* ***a)*** *was obtained from (Danalache et al., 2019a) and is used with the kind approval of Marina Danalache.*

2.3.6. AFM measurement procedure, ECM and PCM measurement locations

In total, 30 patients were analyzed for the AFM stiffness investigation of osteoarthritic cartilage. One tissue sample was prepared per patient. On each tissue sample, for each of the four different spatial patterns (SS, DS, SC, BC), two independent spatial chondrocyte patterns were chosen and measured. At each of the two chosen spatial chondrocyte patterns, one ECM and PCM location was chosen and used for AFM measurement (Figure 10). For PCM measurements, the microsphere of the cantilever tip was positioned directly next to a chondrocyte of the spatial pattern of interest. For ECM measurements, the cantilever tip was placed in close proximity to the measured PCM in a square of

150 µm × 150 µm, at a position at which the presence of cellular components was low (Figure 10).

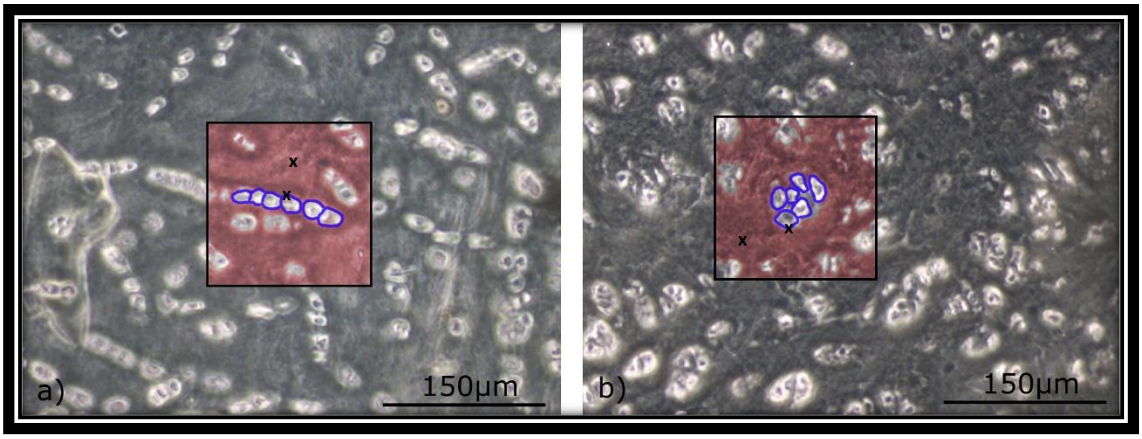

Figure 10. Graphical representation of the AFM measurement method for the ECM (red) and PCM (blue). *Brightfield images showing the chondrocytes in white, embedded in their vast ECM (grey).* The *150 µm × 150 µm square depicts the pre-selected area where the PCM and ECM measurement positions (black crosses) were chosen.* ***a)*** *Shows an exemplary demonstration of the PCM and ECM AFM measurement location of a single string and* ***b)*** *of a small cluster. At each spatial chondrocyte pattern, one position of the ECM and PCM was chosen and measured.*

As preset by the AFM, nine consecutive measurements were conducted at each selected ECM and PCM position. The median of these nine measurements per chosen ECM and PCM position was calculated. This median was then used to calculate the arithmetic mean of the two independent spatial arrangement patterns for each of the four different spatial patterns (SS, DS, SC, BC). This calculation yielded one arithmetic mean value for each matrix (ECM and PCM) for all four spatial chondrocyte patterns per patient. From these values, the arithmetic mean and the median from all 30 patients was calculated for both matrices of each spatial arrangement pattern (SS, DS, SC, BC) (Tables 5 and 6).

The following AFM measurement parameters were used to perform the stiffness measurements: Setpoint = 305.144 nN, Pulling length = 90.0 µm, Extended speed = 5 µm/s, Contact time = 0 sec., Z movement = Constant speed, Delay mode = Constant force, Section rate = 2000 Hz.

2.4. Immunofluorescence staining

2.4.1. Fixation

After the AFM stiffness measurements, the cartilage sections were removed from the tissue culture dish 40 and washed in PBS at room temperature (21°C) for five minutes with the Eppendorf ThermoMixer®. The Eppendorf ThermoMixer® permitted an accelerated washing process of the cartilage samples. Next, the sections were fixed in 4% (v/v) formaldehyde in PBS for 30 minutes at room temperature. Following fixation, sections were washed in PBS three times for five minutes at room temperature using the Eppendorf ThermoMixer®.

2.4.2. Enzyme-induced epitope retrieval

The sections were treated with a 1mg/ml hyaluronidase concentration in PBS for antigen unmasking (Keiser and Hatcher, 1979) to allow a more successful antibody binding. The entire section was covered with hyaluronidase and incubated in the Eppendorf ThermoMixer® at 37°C for one hour. After enzymatic digestion, the sections were washed three times for five minutes at room temperature in the Eppendorf ThermoMixer®.

2.4.3. Blocking

Before antibody application, the sections were blocked to prevent antibody binding to unspecific epitopes. Blocking was achieved by treating the sections with a blocking solution consisting of 0.3% (v/v) Triton X-100 in PBS and 5% (w/v) bovine serum albumin (BSA) in PBS. The sections were incubated with the blocking solution in the Eppendorf ThermoMixer® at 37°C for one hour, then washed three times in PBS for five minutes each.

2.4.4. Primary antibody

Anti-collagen type I (Abcam) and II (Thermo Fisher Scientific) antibodies were used for collagen type I and II staining. Both antibodies were diluted 1:100 with a 2.5% (w/v) BSA in PBS solution. Next, the antibodies were added to the sections, which were subsequently incubated overnight at 4°C. For the negative control, no primary antibodies were applied. Instead, only PBS was added to the sections.

2.4.5. Secondary antibody

Before the secondary antibodies were added, the sections were washed three times in PBS for five minutes. The Alexa Fluor 594 (Abcam) antibody was used as the secondary antibody for collagen type I and II staining, diluted 1:100 with PBS. For nuclear staining, DAPI was used at a working concentration of 1µg/ml. After the dilution had been added to the sections, including sections for the negative control, they were incubated in the Eppendorf ThermoMixer® for two hours at room temperature. Finally, the sections were washed three times for five minutes in PBS.

2.4.6. Section placement on glass slide and microscopic imaging

Fluorescent labeled sections were placed onto glass slides, and a fluorescent mounting medium was added. Lastly, the sections were covered with coverslips. For microscopy and image acquisition, the Zeiss AxioPhot Fluorescent Microscope was used. All images, including positive and negative controls, were taken using the same image parameters: AxioCamMR3, Axiocam Typ: 4105, exposure time (ms): 50.

2.5. Statistical analysis

The AFM stiffness results were compared with the Friedman test, a nonparametric hypothesis test. For post hoc analysis of the chondrocyte pattern comparison, Dunn's test was performed, a nonparametric pairwise multiple comparison test. The Benjamini-Hochberg procedure was performed to correct for multiple testing based on an alpha level = 0.05.

In order to further analyze the relationship of the biomechanical changes in the ECM and the PCM throughout the course of OA, their ECM/PCM ratios were calculated. For this purpose, the ECM/PCM ratio for each patient was first calculated from their corresponding arithmetic mean YM values for each spatial chondrocyte pattern. This calculation yielded an ECM/PCM ratio value for all four spatial chondrocyte patterns for each patient. From the data set generated from these ratio values, the median ECM/PCM ratio for each spatial chondrocyte pattern across all patients was calculated (Table 7 and Figure 12b)). The maximum ratio describes the ECM/PCM ratio of the patient, which showed the highest difference in YM for the ECM compared to the PCM. This description also applies vice versa for the minimum ratio (Table 7). The Spearman's rank correlation coefficient was applied to evaluate the relationship between ECM/PCM ratios with the different chondrocyte patterns. The Spearman's rank correlation coefficient is a nonparametric rank statistical calculation used to determine the strength of an association between two variables (Hauke and Kossowski, 2011). The present study examined the cellular organization pattern and ECM/PCM ratio as variables. Statistical analysis was performed with IBM SPSS Statistics 22 (IBM Corp., Armonk, NY, USA) and Microsoft Excel 2016.

3. Results

3.1. AFM

From each of the 30 patients, two independent chondrocyte patterns were measured for each of the four different chondrocyte patterns (SS, DS, SC, BC), which yielded in the examination of 60 single strings, 60 double strings, 60 small clusters, and 60 big clusters. Thus, 4320 AFM measurements were conducted in total, 2160 for the ECM and PCM, respectively.

The median YM was 132 (44-472) kPa for the ECM and 65 (28-224) kPa for the PCM in healthy cartilage areas, represented by single strings, which showed that the stiffness was more than twice as high in the ECM compared to the PCM. For double strings, which are increasingly present at the onset of OA, the median YM for the ECM was 99 (17-308) kPa and 47 (9-150) kPa for the PCM. The YM values of the other spatial chondrocyte patterns, which demonstrate the later stages of OA, showed a similar trend. Small clusters showed a YM for the ECM of 48 (13-106) kPa and a YM for the PCM of 28 (2-70) kPa. Big clusters, present in joint areas with severe tissue destruction, showed the lowest stiffness with a YM for the ECM of 18 (3-64) kPa and a YM for the PCM of 13 (1-38) kPa (Tables 5 and 6, Figures 11 and 12a)).

After application of the Benjamini-Hochberg FDR correction (alpha = 0.05), significant stiffness reductions were observable throughout all spatial chondrocyte organization changes for both matrices by means of the Friedman test, the only exception being the comparison of single strings to double strings (SS-DS) for ECM values ($p = 0.072$) (Table 8). The YM measurements showed that the mean ECM and PCM stiffness decreases continuously with advancing osteoarthritic tissue degeneration characterized by chondrocyte spatial organization changes (Figure 12 a)). However, the median ECM/PCM ratio remained mostly unchanged (Figure 12 b)). A slight reduction in the ECM/PCM ratios was observable from double strings (2.030) to single strings (2.006) to small clusters (1.938) to big clusters (1.745) (Table 7). The Spearman's rank correlation coefficient demonstrated a slight inverse correlation between the

ECM/PCM ratio and the cellular pattern. However, no significant changes were identified ($r = -0.099$, $p = 0.281$).

Table 5. Young's modulus values of the ECM as assessed by AFM for the different spatial chondrocyte patterns. *Abbreviations: SS – single strings, DS – double strings, SC – small clusters, BC – big clusters. Data from this table are already published in (Danalache et al., 2019a) and are used with permission from Elsevier.*

	SS	DS	SC	BC
Arithmetic mean (kPa)	177.37	110.52	52.67	24.33
Median (kPa)	131.67	98.82	47.98	18.47
Standard deviation (kPa)	117.78	67.18	27.37	16.24
Maximum (kPa)	472.18	308.41	106.44	64.08
Minimum (kPa)	44.24	17.12	12.98	2.88
Range (kPa)	427.29	291.29	93.46	61.19

Table 6. Young's modulus values of the PCM as assessed by AFM for the different spatial chondrocyte patterns. *Abbreviations: SS – single strings, DS – double strings, SC – small clusters, BC – big clusters. Data from this table are already published in (Danalache et al., 2019a) and are used with permission from Elsevier.*

	SS	DS	SC	BC
Arithmetic mean (kPa)	82.36	57.92	28.29	14.21
Median (kPa)	65.23	46.67	28.07	13.00
Standard deviation (kPa)	51.51	38.45	15.64	10.59
Maximum (kPa)	224.44	149.61	69.73	38.42
Minimum (kPa)	27.56	9.41	2.07	1.27
Range (kPa)	196.88	140.19	67.66	37.15

Table 7. ECM/PCM Young's modulus ratios for the different spatial chondrocyte patterns. *No significant difference was found between the YM ratios of ECM/PCM and spatial chondrocyte changes by means of the Spearman's rank correlation coefficient (p = 0.281). Abbreviations: SS – single strings, DS – double strings, SC – small clusters, BC – big clusters. Data from this table are already published in (Danalache et al., 2019a) and are used with permission from Elsevier.*

	SS	DS	SC	BC
Median ECM/PCM ratio (kPa)	2.01	2.03	1.94	1.75
Maximum ratio(kPa)	7.47	5.26	16.11	6.39
Minimum ratio (kPa)	0.90	1.02	0.91	1.06

Table 8. Inferential analysis (p-values) of Young's modulus measurements for the ECM and PCM between the different spatial chondrocyte patterns. *P-value calculations using the Friedman test were performed after FDR correction (Benjamini-Hochberg procedure) on the basis of alpha = 0.05. Significant p-values are marked in bold. Abbreviations: SS – single strings, DS – double strings, SC – small clusters, BC – big clusters. Data from this table are already published in (Danalache et al., 2019a) and are used with permission from Elsevier.*

Spatial pattern comparison	ECM	PCM
SS-DS	0.072	**0.028**
SS-SC	**<0.001**	**<0.001**
SC-BC	**<0.001**	**<0.001**
DS-SC	**0.001**	**0.002**
DS-BC	**<0.001**	**<0.001**
SC-BC	**0.001**	**0.006**

As the AFM data showed a non-normal distribution, the median was applied to compare ECM and PCM stiffness values within the present study. In addition, the arithmetic mean was calculated and applied so that the comparison with previous literature, which mainly used arithmetic mean stiffness values, is more direct. For graphical presentation, AFM median values are displayed as boxplots (Figure 11) and line charts (Figure 12 a)).

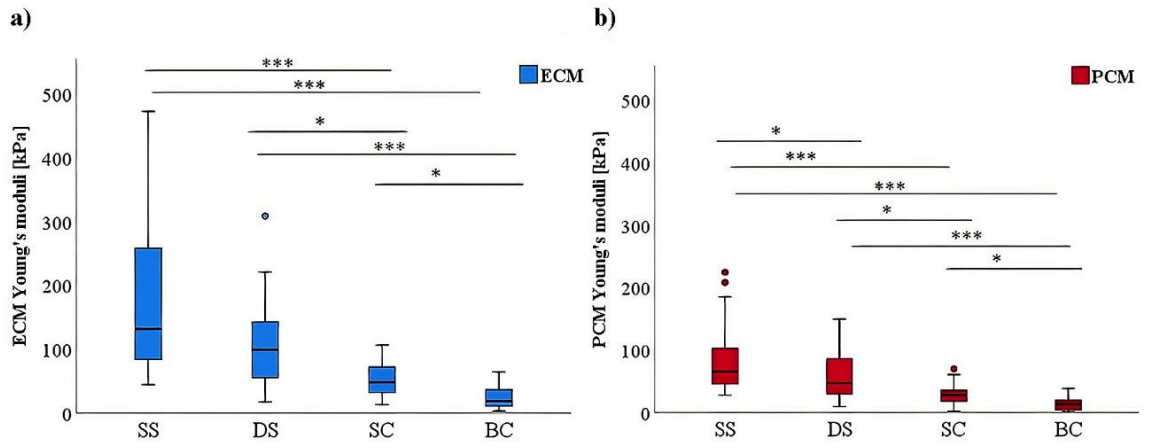

Figure 11. Boxplots illustrating the measured Young's moduli of the a) ECM and b) PCM. *Both boxplots show a decrease in the YM for the ECM and PCM according to the different spatial chondrocyte patterns, representing the progression of osteoarthritic degeneration. * = p < 0.05, *** = p < 0.001 (exact p-values can be viewed in Table 8). Abbreviations: SS – single strings, DS – double strings, SC – small clusters, BC – big clusters. Illustrations were obtained from (Danalache et al., 2019a) and are used with permission from Elsevier.*

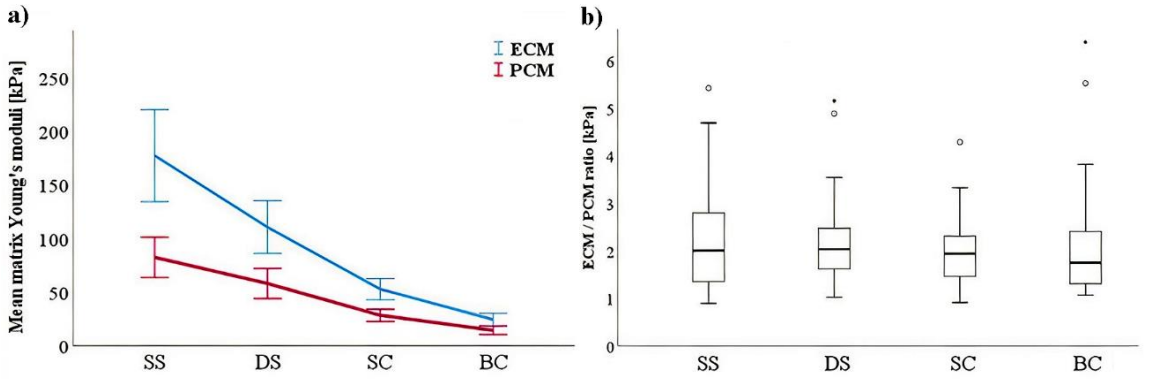

Figure 12. a) Line chart illustrating the mean Young's moduli of the ECM and PCM. b) Boxplot depicting the ECM/PCM ratio for each spatial chondrocyte pattern. a) *The line chart shows a continuous decrease in the YM for the ECM and PCM according to the different spatial chondrocyte patterns, representing the progression of osteoarthritic degeneration.* ***b)*** *The boxplot shows the ECM/PCM ratio for each spatial chondrocyte pattern. No significant difference was found between the ECM/PCM ratio of the different spatial patterns (p = 0.281). Abbreviations: SS – single strings, DS – double strings, SC – small clusters, BC – big clusters. Illustrations were obtained from (Danalache et al., 2019a) and are used with permission from Elsevier.*

3.2. Immunofluorescence microscopy

The immunofluorescence staining aimed to investigate how the intensity and integrity of collagen type I and II staining correlate with OA-related chondrocyte spatial organization changes and the stiffness changes of the ECM and PCM. In the course of OA, where single strings progress to the formation of big clusters, immunofluorescence analysis showed that the staining of collagen type II, which almost entirely makes up the ECM (Akkiraju and Nohe, 2015, Guilak et al., 1999, Lahm et al., 2010, Poole et al., 2002), showed a continuous decrease in signal intensity and integrity (Figures 12-15 a)-c)). Collagen type I, which is typically almost entirely absent in healthy articular cartilage (Roberts et al., 2009), showed an increase in staining intensity (Figures 12-15 d)-f)) as OA progression occurred. Details of these findings are displayed in more detail in the following paragraphs.

3.2.1. Single string immunofluorescence microscopy

Collagen type II staining images of single strings showed a high and evenly distributed staining appearance, as a strong fluorescence signal was visualized throughout the ECM (Figure 13 a)-c)). Conversely, in images where collagen type I staining was conducted, a fluorescence signal was not observable, implying that no relevant amount of collagen type I was present in cartilage areas with single strings (Figure 13 d)-f)).

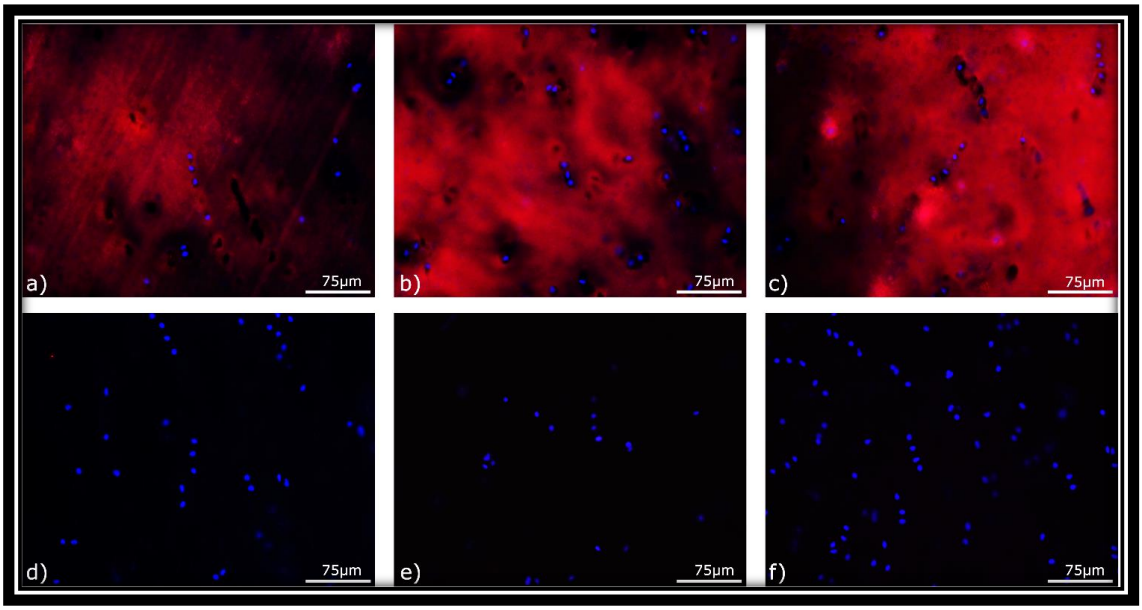

Figure 13. Single string ECM immunofluorescence staining of collagen type II (a)-c)) and collagen type I (d)-f)). *Collagen type II staining is marked by red coloring. Nuclear staining (DAPI) of the chondrocytes can be seen in blue. Single string collagen type II staining shows an intensive and homologous fluorescence signal throughout the ECM (**a)-c)**). Collagen type I staining is not observable in single strings immunofluorescence staining (**d)-f)**).*

3.2.2. Double string immunofluorescence microscopy

The results of double strings were similar to those of single strings. Images of double strings with collagen type II staining showed a moderate fluorescence signal intensity, suggesting that a moderate amount of collagen type II was present in such cartilage areas. It can be noted that the collagen type II staining appearance was slightly more dispersed than the collagen type II staining in single string images (Figure 13 a)-c)), as the red coloring seemed less dense and more discontinuous (Figure 14 a)-c)). No fluorescence signal was observable for the collagen type I staining, which implies that collagen type I was absent (Figure 14 d)-f)).

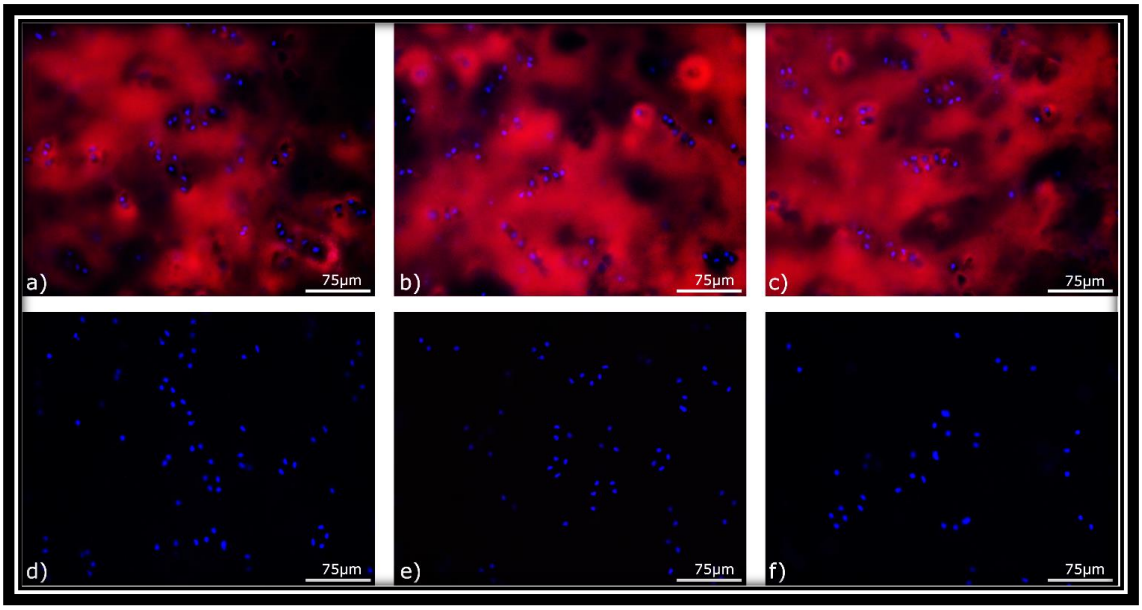

Figure 14. Double string ECM immunofluorescence staining of collagen type II (a)-c)) and collagen type I (d)-f)). *Collagen type II staining is marked by red coloring. Nuclear staining (DAPI) of the chondrocytes can be seen in blue. Double string collagen type II staining shows a moderate fluorescence signal appearance with signal dispersions observable in the ECM (**a)-c)**). Collagen type I staining is absent in double strings immunofluorescence staining (**d)-f)**).*

3.2.3. Small cluster immunofluorescence microscopy

Collagen type II staining images of small clusters showed a fluorescence signal with a lower intensity than that of double strings (Figure 14 a)-c)). It was also clearly visible that the collagen type II staining appearance was more uneven than that of double strings. This uneven distribution was visualized by large areas in the ECM where a fluorescence signal was absent or only with low intensity (Figure 15 a)-c)).

Small clusters were the first chondrocyte spatial pattern where a collagen type I signal was detected. Collagen type I staining signals were absent in less degenerated cartilage areas where OA-related structural changes had not occurred yet or only to a smaller extent, represented by single and double strings (Figures 13 d)-f) and 14 d)-f)). For collagen type I immunofluorescence labeling of small clusters, an intense fluorescence signal could be observed in the ECM (Figure 15 d)-f)).

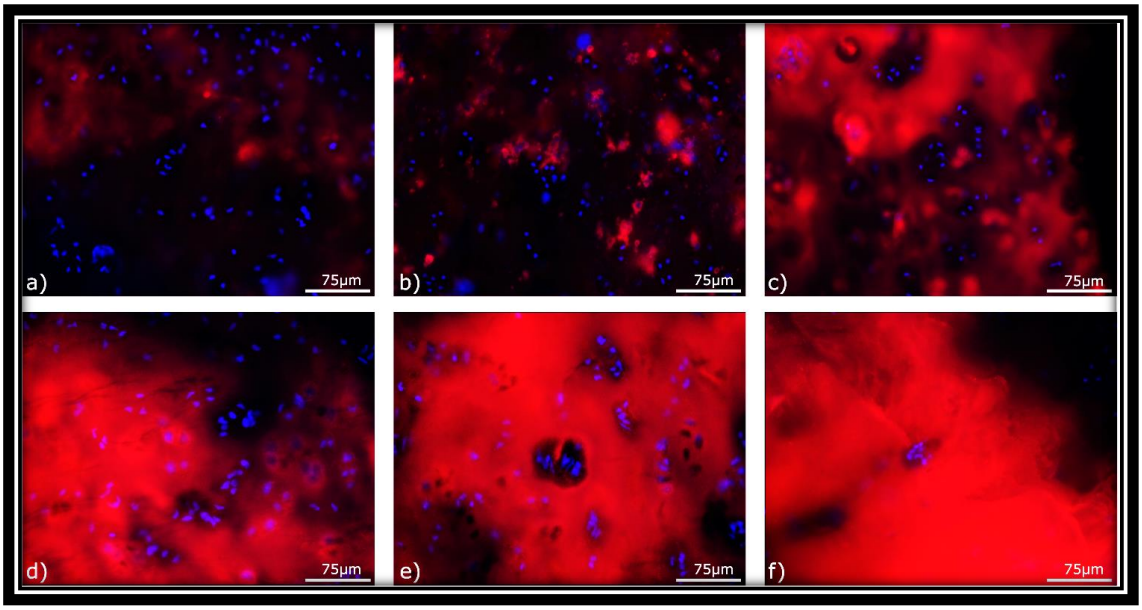

Figure 15. Small cluster ECM immunofluorescence staining of collagen type II (a)-c)) and collagen type I (d)-f)). *Collagen type II and I staining is marked by red coloring. Nuclear staining (DAPI) of the chondrocytes can be seen in blue. Small cluster collagen type II staining shows a reduced fluorescence signal appearance with an uneven distribution throughout the ECM (**a)-c)**). Collagen type I staining of small clusters shows a moderate fluorescence signal appearance with zonal variations in the staining appearance (**d)-f)**).*

3.2.4. Big cluster immunofluorescence microscopy

Collagen type II staining signals of big clusters implied that collagen type II was only present in the ECM to a minimal extent, as only a low fluorescence signal appearance was present. This signal was, moreover, highly disorganized throughout the ECM (Figure 16 a)-c)). In collagen type I staining images of big clusters, a moderate fluorescence signal intensity, similar to that of small clusters (Figure 16 d)-f)), was observed. However, areas surrounding the big cluster with absent collagen type I staining could also be observed (Figure 16 d)-f)).

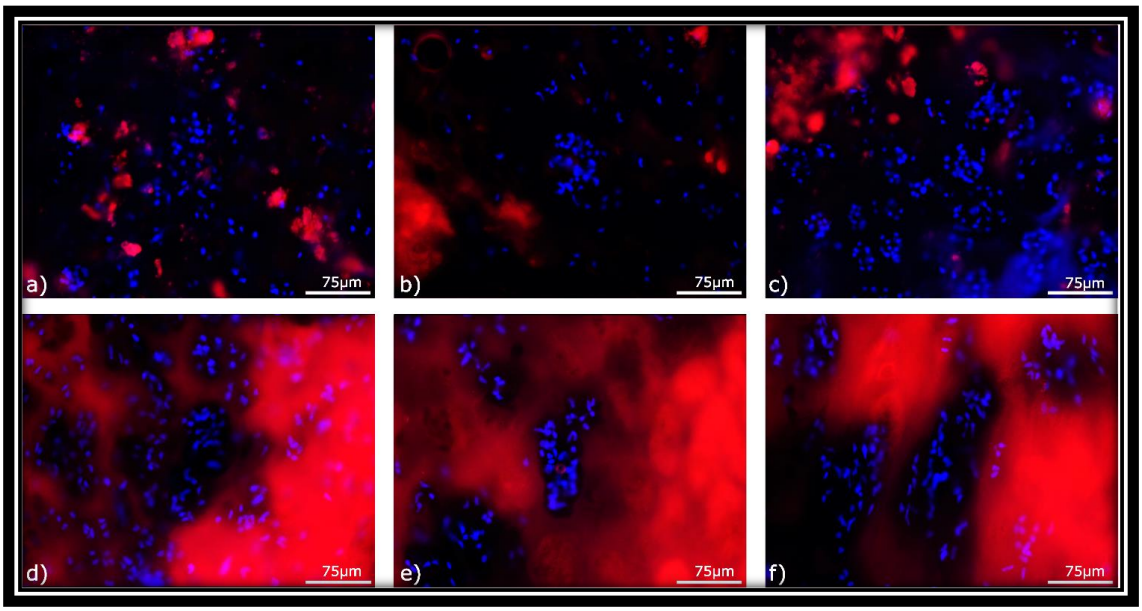

Figure 16. Big cluster ECM immunofluorescence staining of collagen type II (a)-c)) and collagen type I (d)-f)). *Collagen type II and I staining is marked by red coloring. Nuclear staining (DAPI) of the chondrocytes can be seen in blue. Big cluster collagen type II staining shows a weak and scattered fluorescence signal appearance (**a)-c)**). Collagen type I staining of small clusters shows a moderate fluorescence signal appearance with zonal variations in the staining appearance (**d)-f)**).*

3.2.5. Controls for immunofluorescence

The negative controls of collagen type II (a)) and collagen type I (b)) provided evidence that no unspecific antibody binding had occurred. Only the nuclear staining using DAPI was visible in the images, while no other fluorescence signal was detected.

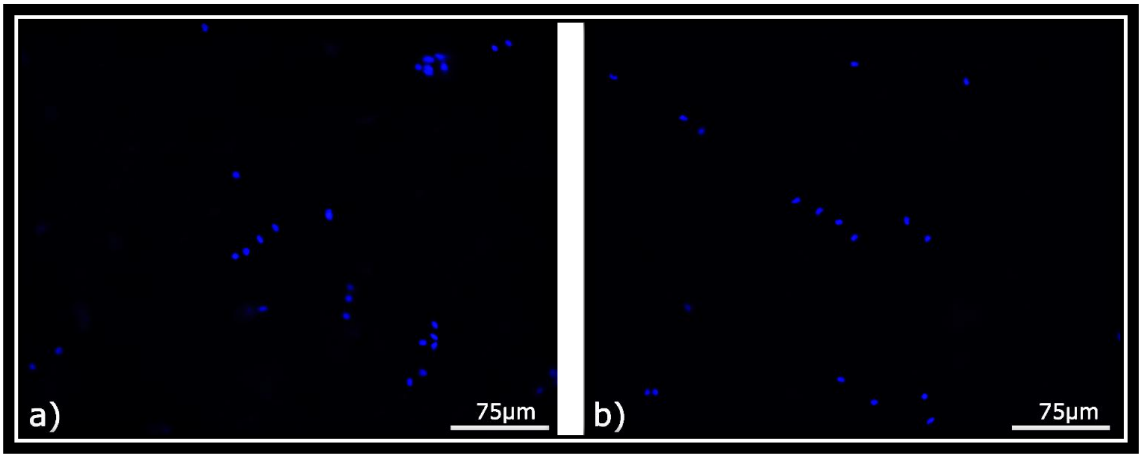

Figure 17. Representative negative controls of ECM immunofluorescence staining of collagen type II (a)) and collagen type I (b)). *Nuclear staining (DAPI) of chondrocyte single strings can be seen in blue.*

4. Discussion

4.1. General overview

OA is considered the most frequent form of arthritis and affects millions worldwide. Because of the high prevalence, OA is an important limiting factor for overall quality of life. Chronic pain and physical disability caused by OA are the main contributors to this limitation in quality of life. It is believed to originate from a complex interplay of various components, such as biomechanic, genetic, metabolic, and biochemical factors (Wilusz et al., 2013, Man and Mologhianu, 2014, Hassanali and Oyoo, 2011).

The precise molecular pathomechanisms of OA are still unknown. However, chondrocyte-mediated inflammatory responses are believed to play a central role in the pathogenesis (Konttinen et al., 2012, Chen et al., 2017a). The onset and progression of OA are thought to be based on a cascade of pathologic events which involve a disbalance of synthesis and degradation of ECM and PCM components. This disequilibrium ultimately contributes to a predominance of proinflammatory cytokines, which promote collagen degradation in the articular cartilage. The increased collagen breakdown causes an alteration of cartilage biomechanical properties and thereby limits the cartilage functions, such as load transmission and shock absorption (Hassanali and Oyoo, 2011). The diagnosis of OA is based on the patient history, clinical examination, and radiography (Arya and Jain, 2013). These diagnostic components are the basis for the indication of an individually chosen and adjusted therapy strategy for the patient.

The initially advised non-surgical therapy helps patients to cope with the emerging symptoms of OA but does not address the degenerative aspect of the disease itself. If a conservative therapy approach proves unsuccessful, surgical interventions such as total knee replacement are often the only option remaining to treat the patient (Katz et al., 2010, Akkawi et al., 2015). A deeper insight into the underlying pathomechanisms of OA is necessary to improve therapy options and to develop further diagnostic procedures to allow early disease detection and to thus help prevent cartilage degeneration at an early stage.

The primary purpose of the present study was to assess stiffness changes of the ECM and PCM in healthy cartilage areas and at different stages of OA cartilage degeneration. The pattern of spatial chondrocyte organization served as a staging method to delineate healthy from early to progressively degenerated cartilage (Rolauffs et al., 2010, Felka et al., 2016, Danalache et al., 2019b). Secondarily, using immunofluorescence staining, the ECM components collagen type I and II were analyzed qualitatively in relation to changes in spatial chondrocyte organization and matrix stiffness. The additional collagen immunohistochemistry served to analyze the relationship between structural protein appearance and matrix stiffness in healthy cartilage areas and at different stages of OA progression.

4.2. AFM data analysis

4.2.1. Overview of Young's modulus data in previous research

In order to evaluate the AFM data of the present research, it was compared to stiffness measurements found in prior literature, which also analyzed healthy and osteoarthritic cartilage. In prior research, AFM investigations of OA-related cartilage stiffness changes yielded mean YM values for the ECM, which ranged from 306 (± 133) kPa (Darling et al., 2010) to 491 (± 112) (Wilusz et al., 2013) kPa in healthy cartilage. In comparison, osteoarthritic cartilage, measured by AFM, showed a lower YM of 270 (± 76) (Wilusz et al., 2013) kPa for the ECM.

Other studies, which previously investigated the YM for the PCM with the micropipette aspiration technique, described mean YM values for the PCM of 40 (± 14) (Alexopoulos et al., 2005) kPa to 69 (± 19) (Alexopoulos et al., 2003) kPa in healthy cartilage. In comparison, osteoarthritic cartilage yielded in mean YM values for the PCM of 21 (± 10) (Alexopoulos et al., 2005) kPa to 40 (± 20) (Alexopoulos et al., 2003) kPa with the micropipette aspiration technique. In later research with AFM application, YM values for the PCM of 104 (± 51) kPa (Darling et al., 2010) to 137 (± 22) kPa (Wilusz et al., 2013) were described in healthy

cartilage. With present osteoarthritic changes, the AFM technique yielded YM values for the PCM of 96 (± 16) kPa (Wilusz et al., 2013).

4.2.2. Comparison of ECM and PCM stiffness measurements with previous research

In the present study, the mean YM for the ECM of healthy cartilage areas represented by single strings was 177 (44-472) kPa (Table 5). The PCM of healthy cartilage areas measured a YM of 82 (28-224) kPa (Table 6). When comparing the YM of both matrices in healthy cartilage areas, the YM for the PCM shows a 54% lower stiffness than the YM for the ECM. In contrast, previous studies showed a PCM to ECM stiffness difference in healthy cartilage of 72% (Wilusz et al., 2013) or 66% (Darling et al., 2010), demonstrating a greater PCM to ECM stiffness difference in healthy cartilage in comparison to that of the present study. These observed differences are, however, still of the same order of magnitude. Given the complexity of the AFM technique and the multiple confounding factors which can affect the outcome of the stiffness measurements, these different studies thus all describe the same principle: that the YM for the ECM is around two- to three-fold higher than that for the PCM.

The main focus of the present study was to evaluate ECM and PCM stiffness changes in the course of cartilage degeneration using spatial chondrocyte organization as a grading system for the severity of the disease. In the present study, the mean YM for the ECM decreased from 177 (44-472) kPa in healthy cartilage areas, represented by single strings, to 24 (3-64) kPa in cartilage areas with severely damaged by OA, represented by big clusters (Table 5). In comparison, the mean YM for the PCM decreased from 82 (28-224) kPa in healthy cartilage areas to 14 (1-38) kPa in cartilage areas severely damaged by OA (Table 6). Overall, this describes a stiffness reduction of 86% for the ECM and 83% for the PCM, as spatial chondrocyte organization advanced from single strings to big clusters. Previous studies only described an ECM stiffness reduction of 45% and a PCM stiffness reduction of 30% in healthy cartilage compared to osteoarthritic cartilage, measured with AFM (Wilusz et al., 2013).

With the micropipette aspiration technique, a PCM stiffness reduction of 43% (Alexopoulos et al., 2003) and 48% (Alexopoulos et al., 2005) was previously described in healthy cartilage compared to osteoarthritic cartilage. Therefore, the cartilage stiffness reduction related to osteoarthritic changes presented itself as slightly more pronounced in the present research than in previous studies. The following paragraphs elaborate on possible causes for the stiffness data differences between the present and previous studies.

4.2.3. Possible explanations for data differences to previous studies

In the previous studies which also used AFM, mainly macroscopic evaluations of cartilage were applied to define the tissue as either healthy (non-OA) or osteoarthritic (OA). For instance, Wilusz et al. used the Collins grading, a macroscopic classification system based on the evaluation of surface fibrillations and fissures (Wilusz et al., 2013). Darling et al. investigated tissue samples characterized as macroscopically healthy regions of the knee joint cartilage (Darling et al., 2010). In the studies by Alexopoulos et al., where the micropipette aspiration technique was applied, a semi-quantitative histologic grading system was used based on the gross appearance of the cartilage, surface fibrillation, specific staining methods, and chondrocyte proliferation (Alexopoulos et al., 2003, Alexopoulos et al., 2005). In contrast, the present study used spatial chondrocyte organization as a classification system which allows the differentiation of several subclasses, which gradually describe different magnitudes of OA-related changes.

It is thus highly conceivable that in those previous studies, due to the primarily macroscopic cartilage evaluation, even in measured tissue that was classified as advanced OA, areas with focally higher and sometimes lower degeneration were measured. This might have leveled the results. As single strings can lie in close proximity to small or even big clusters, only measuring in such a specific way as in the present study allows to precisely describe the local biomechanic properties characteristic for the different spatial patterns. Of note, the values generated in

the present study do thus not describe stiffness values for a macroscopic degeneration grade but are indeed pattern-specific.

Another interesting aspect that can be pointed out is that with a macroscopic classification approach, cartilage is only described as osteoarthritic when the degeneration has occurred to such an extent that it can be detected macroscopically. Cartilage degeneration to a smaller extent is therefore not taken into consideration, and the cartilage could still be regarded as healthy (non-OA) even if earlier degeneration stages are already present. This aspect could also explain why the OA-related ECM and PCM stiffness reduction was only observable to a smaller extent in the previous studies (Alexopoulos et al., 2005, Alexopoulos et al., 2003, Wilusz et al., 2013, Darling et al., 2010) compared to that of the present study.

4.2.4. Evaluation of ECM and PCM stiffness based on spatial chondrocyte organization

In the course of OA, a pronounced and continuous reduction in the YM could be observed for both the ECM and the PCM (Tables 5 and 6, Figures 11 and 12a)). The stiffness reduction presented itself as gradual for both matrices with ongoing spatial chondrocyte organization changes (Figure 12a). This stiffness reduction of the cartilage matrices suggests that as OA-related alterations of spatial chondrocyte organization occur, both the immediate surrounding of the chondrocyte (the PCM) (Danalache et al., 2019b) and the surrounding ECM are impacted in a similar manner. This was also further confirmed when calculating the ECM/PCM ratios for the different spatial patterns, where almost no difference between the different OA stages could be observed. These findings imply that OA affects the ECM and PCM simultaneously and to a comparable extent. Because of that, one can speculate that the degenerative process of the ECM and PCM are of the same origin and underly the same destructive pathophysiological mechanism.

In previous research, Wilusz et al., however, described PCM/ECM stiffness ratios, which increased from 0.36 (± 0.06) in macroscopically healthy cartilage to 0.56 (± 0.13) in osteoarthritic cartilage (Wilusz et al., 2013). These findings imply that as healthy cartilage becomes progressively damaged by OA, the ECM stiffness seems to be impacted more by degenerative changes, or rather that the PCM presents itself as more stable in the course of OA.

It needs to be pointed out that several technical and methodical differences exist between the present study and that of Wilusz et al. that could be related to the differences between the observed ECM/PCM ratios. As aforementioned, in contrast to the present study, Wilusz et al. graded the cartilage as either healthy or osteoarthritic based on the macroscopic Collins grading, and an OA stage subdivision was not applied. In contrast, in the present study, each YM measurement value was obtained from a tissue site that was in direct relation to a specific spatial chondrocyte pattern. Such an allocation would not be the case in a measurement procedure where grading is simply based on macroscopic tissue evaluation.

In addition, several AFM configurations differed between the study of Wilusz et al. and the present study. For instance, Wilusz et al. used a setpoint for the stiffness measurements of approx. 750 nN, whereas in the present study, a setpoint of approx. 305 nN was used. Varying setpoints implicate that different amounts of physical force are applied during measurement, causing different deformation of the sample surface, which could impact the obtained YM data.

Also, the cartilage section preparation differed between the present study and that of Wilusz et al., where, for instance, the cartilage cryosections were five µm thick, whereas, in the present study, cartilage samples were sectioned into 35 µm thick sections. Section thickness is an especially relevant parameter, as the measurement of the ECM follows different technical prerequisites compared to those of the PCM. While the former is a measurement on collagen fibers that are mostly tightly packed next to each other (Fox et al., 2009), the PCM is a spherical structure with collagen fibers that are arranged in a cocoon-like fashion. Since the thickness of the PCM is approximately only 2-4 µm (Guilak et al., 2018), hitting

this narrow structure with the cantilever microsphere also always implies that for the AFM measurement, a chondrocyte with its surrounding PCM lies directly at the section surface which is a factor influenced by the section thickness. Such a phenomenon does not exist for ECM measurements, and section thickness plays a smaller role here. Such methodical differences need to be considered as they may affect the cartilage stiffness measurement procedure and, therefore, the ECM/PCM ratio calculations.

Although the findings of the present study further support a connection between spatial chondrocyte organization changes and osteoarthritic tissue destruction, they do not predict a direct correlation between the events or provide information about the causality of both phenomena. It can only be speculated that OA-related matrix degeneration is a prerequisite for alterations of spatial chondrocyte organization to occur. However, both phenomena could also be occurring autonomously and separately.

OA-related changes in spatial chondrocyte organization have already been described in previous literature (Aicher and Rolauffs, 2014, Felka et al., 2016, Rolauffs et al., 2008). However, these studies did not characterize the distinct functional relevance of chondrocyte organization alteration in detail. The present study is the first to describe cartilage stiffness changes of the ECM and PCM in regard to OA-related changes in spatial chondrocyte organization. The findings of the present study further indicate the efficiency of spatial chondrocyte organization as a biomarker for local OA cartilage degeneration, which with further research, could possibly be integrated into instrument-based methods for the detection of early OA-related changes.

4.3. Immunofluorescence microscopy analysis

4.3.1. Structural protein analysis of the ECM

Using immunohistochemistry, ECM protein analysis was conducted to further assess the relationship between OA-related matrix alterations and chondrocyte spatial organization changes. A prior study by Danalache et al. (Danalache et al.,

2019b) investigated OA-related PCM stiffness changes and alterations in the composition and quantity of main PCM matrix components such as collagen type VI and perlecan (Poole et al., 1992, Youn et al., 2006, Melrose et al., 2008). In the research by Danalache et al., spatial chondrocyte organization also served as an image-based biomarker for the severity of OA, while the YM for the PCM was measured using AFM. The study described that with OA progression, a decrease in stiffness of the PCM was measured while simultaneously changes in staining localization and intensity could be observed predominately for collagen type VI and partially for perlecan, suggesting an interconnection between these two events (Danalache et al., 2019b).

In order to evaluate how two main structural proteins of the ECM qualitatively alter in the course of OA, immunohistochemistry analysis of collagen type I and type II was conducted using spatial chondrocyte organization to grade OA progression. Previous studies have stated that collagen type I mainly appears in osteoarthritic cartilage and only exists to a minor extent in healthy cartilage. In contrast, collagen type II, the main component of the ECM, is present in both healthy and osteoarthritic cartilage (Miosge et al., 2004, Maldonado and Nam, 2013, Lahm et al., 2010, Akkiraju and Nohe, 2015, Guilak et al., 1999, Poole et al., 2002). It has been suggested that the amount of collagen type II decreases with ongoing OA progression and is replaced by collagen type I. Due to the reduction of collagen type II in the course of OA, the mechanical stability and the integrity of the ECM decreases (Maldonado and Nam, 2013, Poole et al., 2002).

4.3.2. Evaluation of ECM immunofluorescence in relation to spatial chondrocyte organization

The results of the present study suggest that in the course of progressive osteoarthritic cartilage degeneration, the integrity and abundance of collagen type II progressively decreases from one spatial chondrocyte pattern to the following (Figures 13-16). The changes in collagen type II appearance and spatial chondrocyte organization were accompanied by a continuous cartilage stiffness reduction detected by AFM (Figure 11 a) and Figure 12 a)).

Immunohistochemical changes were already detected in the early stages of OA. The ECM of double strings (Figure 14) showed a slightly less regularly distributed collagen type II staining appearance than the staining of single strings (Figure 13). Collagen type II staining of small clusters was more scattered throughout the ECM (Figure 15) than staining of double strings (Figure 14). This trend continued in big cluster staining, where collagen type II staining appeared even further dispersed. Positive collagen type I staining was only detectable in the late stages of OA, represented by small (Figure 15) and big clusters (Figure 16). The results of both spatial chondrocyte patterns (SC, BC) were similar, where collagen type I staining showed a strong intensity and a mostly even distribution in the ECM.

The immunofluorescence analysis further supports the assumption that as OA impacts the articular cartilage progressively, a distinct collagen remodeling occurs, where collagen type II of the ECM decreases and collagen type I becomes more prominent (Lahm et al., 2010, Maldonado and Nam, 2013). The immunofluorescence and AFM results also suggest a correlation between ECM stiffness loss and reduction in collagen type II abundance and integrity. This correlation underlines the critical role of collagen type II as a biomechanical stabilizer of the ECM. However, the exact role of collagen type I in the course of OA has not been identified yet. Further studies are necessary to reveal the precise interaction between collagen remodeling and stiffness reduction of the ECM.

It has previously already been described that the collagen type II of the ECM is essential for the normal mechanical functioning of the articular cartilage and that the thickness of the collagen fibers correlates with the tensile strength of the tissue (Eyre, 1991, Tschaikowsky et al., 2022). From this, the assumption can be made that an OA-related quantitative reduction of collagen type II and a collagen fiber decay into thinner fibrils may directly be responsible for the matrix stiffness reduction observable in the course of OA. Further, the collagen fibrillar network of the ECM provides a cohesive framework necessary for proteoglycan entrapment (Eyre, 1991). It has also been described that proteoglycans, especially aggrecan, are critical for the articular cartilage to resist compressive loads (Fox et al., 2009). From this, it can be speculated that an impaired

proteoglycan functioning due to the collagen type II reduction is linked to a decline of mechanical properties of the articular cartilage, notable through a matrix stiffness reduction.

4.4. Limitations

4.4.1. AFM precision and sensitivity

AFM has proven itself as a highly efficient method to examine the topography, morphology, and mechanical properties of various materials (Desrochers et al., 2010, Imer et al., 2009b, Park et al., 2004, Park et al., 2009, Tomkoria et al., 2007, Qian and Zhao, 2018). Nevertheless, the precision and sensitivity of AFM must be considered when absolute values are interpreted and compared with YM data from other research. Properties and calibration of the cantilever, the individual spring constant, and the attached microsphere play a critical role in the outcome of the measurements (Qian and Zhao, 2018, Stolz et al., 2004). Although AFM is a measurement technique impacted by various methodical parameters, as these were kept constant during the present study, comparison and interpretation of values within the study should be unaffected.

4.4.2. Method of cartilage preparation

The cartilage preparation technique is another factor that impacts the AFM measurements and needs to be considered when YM data are compared with that of other research. The period from the cartilage harvest to the stiffness measurements, the used conserving medium, and the cartilage sectioning method influence the YM results as the validity of the measurements is related to the material homogeneity and surface properties (Qian and Zhao, 2018). As these preparation parameters were kept uniform in the study, the data interpretation and comparison within the study should, however, not be affected.

4.4.3. Specimen selection and cartilage sample evaluation

All AFM measurements in the present study were of diseased knee joints from patients diagnosed with severe OA, whereas articular cartilage of completely healthy knee joints was not examined. It is possible that AFM measurements of single strings, which represent healthy cartilage areas, would differ in biomechanical properties from single string measurements of completely undamaged articular cartilage. It can be assumed that although cartilage areas appeared intact and healthy in terms of spatial chondrocyte organization in the present study, degenerative changes were possibly already present. As OA-related inflammation is already present in early disease stages (Chen et al., 2017a, Loeser et al., 2012), degenerative processes may affect the cartilage matrix even if single strings can still be observed. From these aspects, the assumption can be made that YM values for the ECM and PCM of single strings would be higher in articular cartilage of healthy knee joints than in knee joints affected by OA.

Furthermore, it needs to be pointed out that cartilage sections that predominantly contained healthy cartilage areas, represented by single strings, were probably obtained directly from or near the original cartilage surface, i.e., from the superficial zone. However, cartilage sections with predominantly severe OA degeneration, represented by small and big clusters, were possibly obtained from subjacent cartilage layers such as the middle or deep zone and not from the original cartilage surface. The exposure of deeper cartilage zones is possible when overlying cartilage layers have already been degraded by excessive wear and inflammatory processes of OA. It has been described that the YM increases from the superficial zone toward the deep zone, possibly due to different prevailing collagen types and collagen arrangement (Antons et al., 2018, Chen et al., 2001, Fox et al., 2009). Thereby, the depth of the cartilage layer from which the section was obtained influences the EM, which was another factor that could not be regulated entirely in the cartilage preparation of the present study, as the extent of cartilage surface degeneration varied between the cartilage samples.

Lastly, it needs to be mentioned that biomechanical properties of articular cartilage depend on the anatomical cartilage region of the knee joint. Regional stiffness variations may be explained by differences in the physiological load-bearing demands present in different joint regions (Li et al., 2021). In the present study, the articular cartilage of the weight-bearing zone of the distal femur was investigated. It was not differentiated if cartilage was obtained from the medial or the lateral femur condyle where regional stiffness variations seem to exist. However, the compressive properties between these two joint regions do not differ considerably (Li et al., 2021). Therefore, they should only have a minor impact on the stiffness variation between the joint regions. Nevertheless, a more specific subdivision of the different cartilage joint regions should be considered in future research to increase the validity of cartilage stiffness investigations.

5. Conclusion

OA is one of the most common joint pathologies worldwide, characterized by progressive cartilage degeneration, causing chronic pain and physical disability (Palazzo et al., 2016, Hassanali and Oyoo, 2011). The OA-related collagen destruction of the cartilage alters its biomechanical properties and consequently limits the cartilage function in load transmission and shock absorption, which is necessary for its physiological functioning (Hassanali and Oyoo, 2011). The detailed pathophysiology of OA is only partly understood, which is one reason for the lack of targeted therapy options (Chen et al., 2017a). The present study aimed to investigate biomechanical and structural osteoarthritic changes of human articular cartilage of the knee joint and their relation to changes in spatial chondrocyte organization, which have been suggested as an image-based biomarker for the severity of OA degeneration.

The present study investigated articular cartilage samples of 30 patients diagnosed with advanced knee OA who underwent total knee arthroplasty. Cartilage samples of the femoral condyles were assessed through AFM. Stiffness measurements took place in ECM and PCM regions of the different spatial chondrocyte patterns (SS, DS, SC, BC). Immunofluorescence analysis of collagen type I and II was conducted to evaluate structural changes of both matrices qualitatively.

AFM stiffness measurements showed that changes in the spatial chondrocyte organization strongly correlate with the stiffness of the ECM and PCM. A significant reduction in the stiffness for both matrices with each change of cellular pattern was observed, except for the change from single to double string for the ECM ($p = 0.072$). In the immunofluorescence analysis, collagen type II remodeling into collagen type I could gradually be observed in the course of OA when using spatial chondrocyte organization as an OA biomarker. The present study is the first to describe stiffness changes of the ECM in relation to the PCM and changes in spatial chondrocyte organization quantitatively. The findings imply that OA affects the ECM and PCM simultaneously and to a comparable

extent, suggesting that their degeneration process underlies the same destructive pathophysiological mechanism.

5.1. Zusammenfassung

OA ist eine der häufigsten Gelenkerkrankungen weltweit, die durch Knorpeldegeneration gekennzeichnet ist und chronische Schmerzen sowie körperliche Behinderung verursacht (Palazzo et al., 2016, Hassanali and Oyoo, 2011). Die osteoarthrotisch bedingte Kollagenzerstörung des Knorpels verändert seine biomechanischen Eigenschaften und schränkt somit die Knorpelfunktion bei der Lastübertragung und Stoßdämpfung ein, die für seine physiologische Funktion notwendig sind (Hassanali and Oyoo, 2011). Die detaillierte Pathophysiologie der OA ist nur teilweise verstanden, was einen Grund für den Mangel an zielgerichteter Therapieoptionen darstellt (Chen et al., 2017a). Ziel dieser Arbeit war es, biomechanische und strukturelle osteoarthrotische Veränderungen des menschlichen Gelenkknorpels des Kniegelenks und deren Zusammenhang zu Veränderungen der räumlichen Organisation der Chondrozyten zu untersuchen, welche als bildbasierter Biomarker für den Schweregrad der OA-Degeneration vorgeschlagen wurden.

Die vorliegende Studie untersuchte Gelenkknorpelproben von 30 Patienten, bei denen eine fortgeschrittener Kniearthrose diagnostiziert und eine Knie-Totalendoprothetik durchgeführt wurde. Knorpelproben der Femurkondylen wurden mittels AFM untersucht. Steifigkeitsmessungen fanden in ECM- und PCM-Regionen der verschiedenen räumlichen Chondrozyten-Organisationsmuster (SS, DS, SC, BC) statt. Eine Immunfluoreszenzanalyse von Kollagen Typ I und Typ II wurde durchgeführt, um strukturelle Veränderungen beider Matrices qualitativ zu beurteilen.

Die Steifigkeitsmessungen durch das AFM zeigten, dass Veränderungen in der räumlichen Chondrozytenorganisation stark mit der Steifigkeit von ECM und PCM korrelieren. Eine signifikante Steifigkeitsverringerung für beide Matrizes wurde mit jeder Veränderung des Zellmusters, mit Ausnahme der Veränderung

von Einzel- zu Doppelsträngen in der ECM ($p = 0.072$) beobachtet. In der Immunfluoreszenzanalyse konnte unter Verwendung der räumlichen Chondrozytenorganisation als OA-Biomarker ein gradueller Umbau von Kollagen Typ II zu Kollagen Typ I im Verlauf der OA beobachtet werden. Diese Arbeit beschreibt erstmalig die Steifigkeitsänderungen der ECM in Bezug auf die PCM und Veränderungen der räumlichen Chondrozytenorganisation quantitativ. Die Ergebnisse implizieren, dass OA die ECM und PCM simultan und im vergleichbaren Ausmaß beeinflusst, was darauf hindeutet, dass ihr Degenerationsprozess demselben destruktiven pathophysiologischen Mechanismus unterliegt.

6. Bibliography

ABULHASAN, J. & GREY, M. 2017. Anatomy and Physiology of Knee Stability. *Journal of Functional Morphology and Kinesiology,* 2**,** 1-11.

AICHER, W. K. & ROLAUFFS, B. 2014. The spatial organisation of joint surface chondrocytes: review of its potential roles in tissue functioning, disease and early, preclinical diagnosis of osteoarthritis. *Annals of the Rheumatic Diseases,* 73**,** 645-653.

AKKAWI, I., ERBOSA, V., BRUNI, D., RIZZOLI, I. O., IACONO, F., RIZZOLI, I. O., RASPUGLI, G. F. & RIZZOLI, I. O. 2015. Sports After Total Knee Prosthesis. *Sports Injuries.* Berlin Heidelberg: Springer-Verlag, 2475-2480.

AKKIRAJU, H. & NOHE, A. 2015. Role of Chondrocytes in Cartilage Formation, Progression of Osteoarthritis and Cartilage Regeneration. *Journal of Developmental Biology,* 3**,** 177-192.

ALEXOPOULOS, L. G., HAIDER, M. A., VAIL, T. P. & GUILAK, F. 2003. Alterations in the Mechanical Properties of the Human Chondrocyte Pericellular Matrix With Osteoarthritis. *Journal of Biomechanical Engineering,* 125**,** 323-333.

ALEXOPOULOS, L. G., WILLIAMS, G. M., UPTON, M. L., SETTON, L. A. & GUILAK, F. 2005. Osteoarthritic changes in the biphasic mechanical properties of the chondrocyte pericellular matrix in articular cartilage. *Journal of Biomechanics,* 38**,** 509-517.

ANTONS, J., MARASCIO, M. G. M., NOHAVA, J., MARTIN, R., APPLEGATE, L. A., BOURBAN, P. E. & PIOLETTI, D. P. 2018. Zone-dependent mechanical properties of human articular cartilage obtained by indentation measurements. *Journal of Materials Science: Materials in Medicine,* 29**,** 1-8.

ARYA, R. K. & JAIN, V. 2013. Osteoarthritis of the knee joint: An overview. *Journal, Indian Academy of Clinical Medicine,* 14**,** 154-162.

ATTUR, M., KRASNOKUTSKY-SAMUELS, S., SAMUELS, J. & ABRAMSON, S. B. 2013. Prognostic biomarkers in osteoarthritis. *Current Opinion in Rheumatology,* 25**,** 136-144.

BHOSALE, A. M. & RICHARDSON, J. B. 2008. Articular cartilage: structure, injuries and review of management. *British Medical Bulletin,* 87**,** 77-95.

BRÜCKNER, B. R., NÖDING, H. & JANSHOFF, A. 2017. Viscoelastic Properties of Confluent MDCK II Cells Obtained from Force Cycle Experiments. *Biophysical Journal,* 112**,** 724-735.

CHEN, D., SHEN, J., ZHAO, W., WANG, T., HAN, L., HAMILTON, J. L. & IM, H.-J. 2017a. Osteoarthritis: toward a comprehensive understanding of pathological mechanism. *Bone research,* 5**,** 1-13.

CHEN, S., FU, P., WU, H. & PEI, M. 2017b. Meniscus, articular cartilage and nucleus pulposus: a comparative review of cartilage-like tissues in anatomy, development and function. *Cell and Tissue Research,* 370**,** 53-70.

CHEN, S. S., FALCOVITZ, Y. H., SCHNEIDERMAN, R., MAROUDAS, A. & SAH, R. L. 2001. Depth-dependent compressive properties of normal aged human femoral head articular cartilage: relationship to fixed charge density. *Osteoarthritis and Cartilage,* 9**,** 561-569.

CHEN, Y.-S. 2016. Testing and modeling tensile stress-strain curve for prestressing wires in railroad ties. *Department of Civil Engineering, College of Engineering, Kansas State University, Manhattan***,** 1-114.

CHOI, M.-C., JO, J., PARK, J., KANG, H. K. & PARK, Y. 2019. NF-κB Signaling Pathways in Osteoarthritic Cartilage Destruction. *Cells,* 8**,** 1-21.

DANALACHE, M. 2020. *Biomechanical assessment of osteoarthritic articular cartilage and jaw periosteal cells-based bone constructs.* Doctor of Philosophy, Universtität Tübingen.

DANALACHE, M., BEUTLER, K. R., ROLAUFFS, B., WOLFGART, J. M., BONNAIRE, F. C., FISCHER, S., GREVING, I. & HOFMANN, U. K. 2021. Exploration of changes in spatial chondrocyte organisation in human osteoarthritic cartilage by means of 3D imaging. *Scientific*

Reports, 11**,** 1-11.

DANALACHE, M., JACOBI, L. F., SCHWITALLE, M. & HOFMANN, U. K. 2019a. Assessment of biomechanical properties of the extracellular and pericellular matrix and their interconnection throughout the course of osteoarthritis. *Journal of Biomechanics,* 97**,** 1-5.

DANALACHE, M., KLEINERT, R., SCHNEIDER, J., ERLER, A. L., SCHWITALLE, M., RIESTER, R., TRAUB, F. & HOFMANN, U. K. 2019b. Changes in stiffness and biochemical composition of the pericellular matrix as a function of spatial chondrocyte organisation in osteoarthritic cartilage. *Osteoarthritis and Cartilage,* 27**,** 823-832.

DARLING, E. M., WILUSZ, R. E., BOLOGNESI, M. P., ZAUSCHER, S. & GUILAK, F. 2010. Spatial mapping of the biomechanical properties of the pericellular matrix of articular cartilage measured in situ via atomic force microscopy. *Biophysical Journal,* 98**,** 2848-2856.

DEBIAIS-THIBAUD, M., SIMION, P., VENTÉO, S., MUÑOZ, D., MARCELLINI, S., MAZAN, S. & HAITINA, T. 2019. Skeletal Mineralization in Association with Type X Collagen Expression Is an Ancestral Feature for Jawed Vertebrates. *Molecular Biology and Evolution,* 36**,** 2265-2276.

DESROCHERS, J., AMREIN, M. A. & MATYAS, J. R. 2010. Structural and functional changes of the articular surface in a post-traumatic model of early osteoarthritis measured by atomic force microscopy. *Journal of Biomechanical Engineering,* 43**,** 3091-3098.

EPPELL, S., LIU, Y. & ZYPMAN, F. 2016. Accuracy of AFM force distance curves via direct solution of the Euler-Bernoulli equation. *AIP Advances,* 6**,** 1-9.

EYMARD, F., PARSONS, C., EDWARDS, M. H., PETIT-DOP, F., REGINSTER, J. Y., BRUYÈRE, O., RICHETTE, P., COOPER, C. & CHEVALIER, X. 2015. Diabetes is a risk factor for knee osteoarthritis progression. *Osteoarthritis Cartilage,* 23**,** 851-9.

EYRE, D. R. 1991. The collagens of articular cartilage. *Seminars in Arthritis and Rheumatism,* 21**,** 2-11.

FELKA, T., ROTHDIENER, M., BAST, S., UYNUK-OOL, T., ZOUHAIR, S., OCHS, B. G., DE ZWART, P., STOECKLE, U., AICHER, W. K., HART, M. L., SHIOZAWA, T., GRODZINSKY, A. J., SCHENKE-LAYLAND, K., VENKATESAN, J. K., CUCCHIARINI, M., MADRY, H., KURZ, B. & ROLAUFFS, B. 2016. Loss of spatial organization and destruction of the pericellular matrix in early osteoarthritis in vivo and in a novel in vitro methodology. *Osteoarthritis and Cartilage,* 24**,** 1200-1209.

FLANDRY, F. & HOMMEL, G. 2011. Normal Anatomy and Biomechanics of the Knee. *Sports Medicine and Arthroscopy Review,* 19**,** 82-92.

FOX, A., BEDI, A. & RODEO, S. 2009. The Basic Science of Articular Cartilage: Structure, Composition, and Function. *Sports Health,* 1**,** 461-468.

FOX, A., BEDI, A. & RODEO, S. 2012. The Basic Science of Human Knee Menisci: Structure, Composition, and Function. *Sports Health,* 4**,** 340-351.

FUCHS, J., KUHNERT, R. & SCHEIDT-NAVE, C. 2017. 12-Monats-Prävalenz von Arthrose in Deutschland. *Robert Koch-Institut, Epidemiologie und Gesundheitsberichterstattung,* 2**,** 55-60.

GAO, Y., LIU, S., HUANG, J., GUO, W., CHEN, J., ZHANG, L., ZHAO, B., PENG, J., WANG, A., WANG, Y., XU, W., LU, S., YUAN, M. & GUO, Q. 2014. The ECM-cell interaction of cartilage extracellular matrix on chondrocytes. *BioMed Research International***,** 1-8.

GE, Z., HU, Y., HENG, B. C., YANG, Z., OUYANG, H., LEE, E. H. & CAO, T. 2006. Osteoarthritis and therapy. *Arthritis & Rheumatism* 55**,** 493-500.

GLASER, C. & PUTZ, R. 2002. Functional anatomy of articular cartilage under compressive loading Quantitative aspects of global, local and zonal reactions of the collagenous network with respect to the surface integrity. *Osteoarthritis Cartilage,* 10**,** 83-99.

GLAUBITZ, M., BLOCK, S. & GOTTSCHALK, K. 2011. Gluing micro-spheres on cantilevers in

aqueous solution. *JPK Instruments AG*, 1-2.
GOLDRING, M. B. & OTERO, M. 2011. Inflammation in osteoarthritis. *Current Opinion in Rheumatology,* 23**,** 471-478.
GOLDRING, S. R. & GOLDRING, M. B. 2004. The Role of Cytokines in Cartilage Matrix Degeneration in Osteoarthritis. *Clinical Orthopaedics and Related Research,* 427**,** 27-36.
GUILAK, F., JONES, W. R., TING-BEALL, H. P. & LEE, G. M. 1999. The deformation behavior and mechanical properties of chondrocytes in articular cartilage. *Osteoarthritis and Cartilage,* 7**,** 59-70.
GUILAK, F., NIMS, R. J., DICKS, A., WU, C.-L. & MEULENBELT, I. 2018. Osteoarthritis as a disease of the cartilage pericellular matrix. *Matrix biology : journal of the International Society for Matrix Biology,* 71-72**,** 40-50.
HAN, S. K., FEDERICO, S., GRILLO, A., GIAQUINTA, G. & HERZOG, W. 2007. The Mechanical Behaviour of Chondrocytes Predicted with a Micro-structural Model of Articular Cartilage. *Biomechanics and Modeling in Mechanobiology,* 6**,** 139-150.
HARRIS, J. & FLANIGAN, D. 2011. Management of Knee Articular Cartilage Injuries. *Operative Techniques in Sports Medicine,* 13**,** 103-128.
HASSANALI, S. H. & OYOO, G. O. 2011. Osteoarthritis: A Look at Pathophysiology and Approach to New Treatments: A Review. *East African Orthopaedic Journal,* 5**,** 51-57.
HAUKE, J. & KOSSOWSKI, T. 2011. Comparison of Values of Pearson's and Spearman's Correlation Coefficients on the Same Sets of Data. *Quaestiones Geographicae,* 30**,** 87-93.
HEIDARI, B. 2011. Knee osteoarthritis prevalence, risk factors, pathogenesis and features: Part I. *Caspian Journal of Internal Medicine,* 2**,** 205-212.
HIRSCHMANN, M. & MÜLLER, W. 2015. Complex function of the knee joint: the current understanding of the knee. *Knee Surgery, Sports Traumatology, Arthroscopy.* Berlin: Springer-Verlag, 2780-2788.
HUNTER, D. J. & FELSON, D. T. 2006. Osteoarthritis. *British Medical Journal,* 332**,** 639-642.
IMER, R., AKIYAMA, T., DEROOIJ, N.-F., STOLZ, M., AEBI, U., FRIEDERICH, N. & STAUFER, U. 2009a. Indentation-type atomic force microscopy of porcine articular cartilage using an arthroscopic approach. *Archives of Histology and Cytology,* 72**,** 251-259.
IMER, R., AKIYAMA, T., F. DE ROOIJ, N., STOLZ, M., AEBI, U., F. FRIEDERICH, N. & STAUFER, U. 2009b. The measurement of biomechanical properties of porcine articular cartilage using atomic force microscopy. *Archives of Histology and Cytology,* 72**,** 251-259.
JONES, W. R., TING-BEALL, H. P., LEE, G. M., KELLEY, S. S., HOCHMUTH, R. M. & GUILAK, F. 1999. Alterations in the Young's modulus and volumetric properties of chondrocytes isolated from normal and osteoarthritic human cartilage. *Journal of Biomechanics,* 32**,** 119-127.
JPK INSTRUMENTS AG, J. 2012. *JPK Instruments AG- NanoWizard3 User Manual. SPM Software Release 4.2* [Online]. JPK Instruments. [Accessed 02.05.2020 2020].
JPK INSTRUMENTS AG, J. 2021a. *Determining the Elastic Properties of Biological Samples with AFM* [Online]. JPK Instruments. [Accessed 24.03.2021 2021].
JPK INSTRUMENTS AG, J. 2021b. *A practical guide to AFM force spectroscopy and data analysis* [Online]. JPK Instruments. [Accessed 02.05.2020 2020].
JULKUNEN, P., WILSON, W., JURVELIN, J. S. & KORHONEN, R. K. 2009. Composition of the pericellular matrix modulates the deformation behaviour of chondrocytes in articular cartilage under static loading. *Medical and Biological Engineering and Computing,* 47**,** 1281-1290.
JUNG, H.-J., FISHER, M. B. & WOO, S. L. Y. 2009. Role of biomechanics in the understanding of normal, injured, and healing ligaments and tendons. *Sports Medicine, Arthroscopy, Rehabilitation, Therapy & Technology* 1**,** 1-17.
KATZ, J. N., EARP, B. E. & GOMOLL, A. H. 2010. Surgical management of Osteoarthritis. *Arthritis Care and Research,* 62**,** 1220-1228.

KEISER, H. D. & HATCHER, V. B. 1979. The effect of contaminant proteases in testicular hyaluronidase preparations on the immunological properties of bovine nasal cartilage proteoglycan. *Connect Tissue Research,* 6**,** 229-233.

KEMPSON, G. E., FREEMAN, M. A. R. & SWANSON, S. A. V. 1968. Tensile Properties of Articular Cartilage. *Nature,* 220**,** 1127-1128.

KOHN, M. D., SASSOON, A. A. & FERNANDO, N. D. 2016. Classifications in Brief: Kellgren-Lawrence Classification of Osteoarthritis. *Clinical Orthopaedics and Related Research,* 474**,** 1886-1893.

KONTTINEN, Y. T., SILLAT, T., BARRETO, G., AINOLA, M. & NORDSTRÖM, D. C. E. 2012. Editorial: Osteoarthritis as an autoinflammatory disease caused by chondrocyte-mediated inflammatory responses. *Arthritis & Rheumatism,* 64**,** 613-616.

KOURI, J. B., JIMÉNEZ, S. A., QUINTERO, M. & CHICO, A. 1996. Ultrastructural study of chondrocytes from fibrillated and non-fibrillated human osteoarthritic cartilage. *Osteoarthritis and Cartilage,* 4**,** 111-125.

LAASANEN, M. S., TÖYRÄS, J., KORHONEN, R. K., RIEPPO, J., SAARAKKALA, S., NIEMINEN, M. T., HIRVONEN, J. & JURVELIN, J. S. 2003. Biomechanical properties of knee articular cartilage. *Biorheology,* 40**,** 133-140.

LAHM, A., MROSEK, E., SPANK, H., ERGGELET, C., KASCH, R., ESSER, J. & MERK, H. 2010. Changes in content and synthesis of collagen types and proteoglycans in osteoarthritis of the knee joint and comparison of quantitative analysis with Photoshop-based image analysis. *Archives of Orthopaedic and Trauma Surgery,* 130**,** 557-564.

LEDDY, H. A., CHRISTENSEN, S. E. & GUILAK, F. 2008. Microscale diffusion properties of the cartilage pericellular matrix measured using 3D scanning microphotolysis. *Journal of Biomechanical Engineering,* 130**,** 1-20.

LI, H., LI, J., YU, S., WU, C. & ZHANG, W. 2021. The mechanical properties of tibiofemoral and patellofemoral articular cartilage in compression depend on anatomical regions. *Scientific Reports,* 11**,** 1-10.

LOESER, R. F., GOLDRING, S. R., SCANZELLO, C. R. & GOLDRING, M. B. 2012. Osteoarthritis: a disease of the joint as an organ. *Arthritis & Rheumatology* 64**,** 1697-1707.

LOTZ, M., MARTEL-PELLETIER, J., CHRISTIANSEN, C., BRANDI, M. L., BRUYÈRE, O., CHAPURLAT, R., COLLETTE, J., COOPER, C., GIACOVELLI, G., KANIS, J. A., KARSDAL, M. A., KRAUS, V., LEMS, W. F., MEULENBELT, I., PELLETIER, J. P., RAYNAULD, J. P., REITER-NIESERT, S., RIZZOLI, R., SANDELL, L. J., VAN SPIL, W. E. & REGINSTER, J. Y. 2014. Republished: Value of biomarkers in osteoarthritis: current status and perspectives. *Postgraduate Medical Journal,* 90**,** 171-178.

MABEY, T. & HONSAWEK, S. 2015. Cytokines as biochemical markers for knee osteoarthritis. *World Journal of Orthopedics,* 6**,** 95-105.

MALDONADO, M. & NAM, J. 2013. The role of changes in extracellular matrix of cartilage in the presence of inflammation on the pathology of osteoarthritis. *BioMed Research International,* 1**,** 1-10.

MAN, G. & MOLOGHIANU, G. 2014. Osteoarthritis pathogenesis – a complex process that involves the entire joint. *Journal of Medicine and Life,* 7**,** 37-41.

MASUTANI, T., YAMADA, S., HARA, A., TAKAHASHI, T., GREEN, P. G. & NIWA, M. 2020. Exogenous Application of Proteoglycan to the Cell Surface Microenvironment Facilitates to Chondrogenic Differentiation and Maintenance. *International Journal of Molecular Sciences,* 21**,** 1-22.

MELROSE, J., HAYES, A. J., WHITELOCK, J. M. & LITTLE, C. B. 2008. Perlecan, the "jack of all trades" proteoglycan of cartilaginous weight-bearing connective tissues. *Bioessays,* 30**,** 457-469.

MICHAEL, J. W. P., SCHLÜTER-BRUST, K. U. & EYSEL, P. 2010. The epidemiology, etiology, diagnosis, and treatment of osteoarthritis of the knee. *Deutsches Aerzteblatt Online,*

107**,** 152-162.
MIOSGE, N., HARTMANN, M., MAELICKE, C. & HERKEN, R. 2004. Expression of collagen type I and type II in consecutive stages of human osteoarthritis. *Histochemistry and Cell Biology,* 122**,** 229-236.
NEOGI, T. 2013. The epidemiology and impact of pain in osteoarthritis. *Osteoarthritis and Cartilage,* 21**,** 1145-1153.
NG, H. Y., LEE, A. A. & SHEN, K. X. 2017. Articular Cartilage: Structure, Composition, Injuries and Repair. *JSM Bone and Joint Disseases,* 1**,** 1-6.
OLIVEIRA, I. & LU, R. 2017. Synovial Knee Joint. *Regenerative Strategies for the Treatment of Knee Joint Disabilities.* Berlin: Springer, Cham, 21-29.
ORLOWSKY, E. W. & KRAUS, V. B. 2015. The Role of Innate Immunity in Osteoarthritis. *The Journal of Rheumatology,* 42**,** 363-371.
OSTERGAARD, K., ANDERSEN, C. B., PETERSEN, J., BENDTZEN, K. & SALTER, D. M. 1999. Validity of histopathological grading of articular cartilage from osteoarthritic knee joints. *Annals of the Rheumatic Diseases,* 58**,** 208-213.
OSTERGAARD, K., PETERSEN, J., ANDERSEN, C. B., BENDTZEN, K. & SALTER, D. M. 1997. Histologic/histochemical grading system for osteoarthritic articular cartilage. Reproducibility and validity. *Arthritis & Rheumatism,* 40**,** 1766-1771.
PALAZZO, C., NGUYEN, C., LEFEVRE-COLAU, M.-M., RANNOU, F. & POIRAUDEAU, S. 2016. Risk factors and burden of osteoarthritis. *Annals of Physical and Rehabilitation Medicine,* 59**,** 134-138.
PARK, S., COSTA, K. D. & ATESHIAN, G. A. 2004. Microscale frictional response of bovine articular cartilage from atomic force microscopy. *Journal of Biomechanics,* 37**,** 1679-1687.
PARK, S., COSTA, K. D., ATESHIAN, G. A. & HONG, K. S. 2009. Mechanical properties of bovine articular cartilage under microscale indentation loading from atomic force microscopy. *Proceedings of the Institution of Mechanical Engineers, Part H: Journal of Engineering in Medicine,* 223**,** 339-347.
PETERS, A. E., AKHTAR, R., COMERFORD, E. J. & BATES, K. T. 2018. The effect of ageing and osteoarthritis on the mechanical properties of cartilage and bone in the human knee joint. *Scientific Reports,* 8**,** 1-13.
POOLE, A. R., GUILAK, F. & ABRAMSON, S. B. 2006. Etiopathogenesis of Osteoarthritis. *Osteoarthritis. Diagnosis and Medical/Surgical Management.* Philadelphia, Pennsylvania, USA: Lippincott Williams & Wilkins, 27-49.
POOLE, A. R., KOBAYASHI, M., YASUDA, T., LAVERTY, S., MWALE, F., KOJIMA, T., SAKAI, T., WAHL, C., EL-MAADAWY, S., WEBB, G., TCHETINA, E. & WU, W. 2002. Type II collagen degradation and its regulation in articular cartilage in osteoarthritis. *Annals of the Rheumatic Diseases,* 61**,** 78-81.
POOLE, C. A., AYAD, S. & GILBERT, R. T. 1992. Chondrons from articular cartilage. V. Immunohistochemical evaluation of type VI collagen organisation in isolated chondrons by light, confocal and electron microscopy. *Journal of Cell Science,* 103**,** 1101-1110.
PRITZKER, K. P. H., GAY, S., JIMENEZ, S. A., OSTERGAARD, K., PELLETIER, J. P., REVELL, P. A., SALTER, D. & VAN DEN BERG, W. B. 2006. Osteoarthritis cartilage histopathology: grading and staging. *Osteoarthritis and Cartilage,* 14**,** 13-29.
QIAN, L. & ZHAO, H. 2018. Nanoindentation of Soft Biological Materials. *Micromachines,* 9**,** 2-24.
RAMAN, S., FITZGERALD, U. & MURPHY, J. M. 2018. Interplay of Inflammatory Mediators with Epigenetics and Cartilage Modifications in Osteoarthritis. *Frontiers in Bioengineering and Biotechnology,* 6**,** 1-9.
REVELL, P. A. 2008. The combined role of wear particles, macrophages and lymphocytes in the loosening of total joint prostheses. *Journal of the Royal Society, Interface,* 5**,** 1263-1278.
RIVIN, E. I. 2010. Introduction and Definitions. *In:* RIVIN, E. I. (ed.) *Handbook of Stiffness and*

Damping in Mechanical Design. Fairfield, Connecticut, USA: ASME Press, 52.

ROA, J. J., ONCINS, G., DIAZ, J., SANZ, F. & SEGARRA, M. 2011. Calculation of Young's modulus value by means of AFM. *Recent patents on nanotechnology,* 5**,** 27-36.

ROACH, H. I. & TILLEY, S. 2007. The Pathogenesis of Osteoarthritis. *Bone and Osteoarthritis.* London: Springer-Verlag, 1-18.

ROBERTS, S., MENAGE, J., SANDELL, L. J., EVANS, E. H. & RICHARDSON, J. B. 2009. Immunohistochemical study of collagen types I and II and procollagen IIA in human cartilage repair tissue following autologous chondrocyte implantation. *The Knee,* 16**,** 398-404.

ROLAUFFS, B., ROTHDIENER, M., BAHRS, C., BADKE, A., WEISE, K., KUETTNER, K. E., KURZ, B., AURICH, M., GRODZINSKY, A. J. & AICHER, W. K. 2011. Onset of preclinical osteoarthritis: The angular spatial organization permits early diagnosis. *Arthritis & Rheumatism,* 63**,** 1637-1647.

ROLAUFFS, B., WILLIAMS, J. M., AURICH, M., GRODZINSKY, A. J., KUETTNER, K. E. & COLE, A. A. 2010. Proliferative remodeling of the spatial organization of human superficial chondrocytes distant from focal early osteoarthritis. *Arthritis & Rheumatism,* 62**,** 489-498.

ROLAUFFS, B., WILLIAMS, J. M., GRODZINSKY, A. J., KUETTNER, K. E. & COLE, A. A. 2008. Distinct horizontal patterns in the spatial organization of superficial zone chondrocytes of human joints. *Journal of Structural Biology,* 162**,** 335-344.

RÖNN, K., REISCHL, N., GAUTIER, E. & JACOBI, M. 2011. Current surgical treatment of knee osteoarthritis. *Arthritis,* 2011**,** 1-9.

RUSTENBURG, C. M. E., EMANUEL, K. S., PEETERS, M., LEMS, W. F., VERGROESEN, P. A. & SMIT, T. H. 2018. Osteoarthritis and intervertebral disc degeneration: Quite different, quite similar. *JOR Spine,* 1**,** 1-10.

SAAVEDRA, M. Á., NAVARRO-ZARZA, J. E., VILLASEÑOR-OVIES, P., CANOSO, J. J., VARGAS, A., CHIAPAS-GASCA, K., HERNÁNDEZ-DÍAZ, C. & KALISH, R. A. 2012. Clinical anatomy of the knee. *Reumatología Clinica,* 8**,** 39-45.

SCHUMACHER, B. L., SU, J. L., LINDLEY, K. M., KUETTNER, K. E. & COLE, A. A. 2002. Horizontally oriented clusters of multiple chondrons in the superficial zone of ankle, but not knee articular cartilage. *The Anatomical Record,* 266**,** 241-248.

SINUSAS, K. 2012. Osteoarthritis: diagnosis and treatment. *American Family Physician,* 85**,** 49-56.

STOLZ, M., GOTTARDI, R., RAITERI, R., MIOT, S., MARTIN, I., IMER, R., STAUFER, U., RADUCANU, A., DÜGGELIN, M., BASCHONG, W., DANIELS, A. U., FRIEDERICH, N. F., ASZODI, A. & AEBI, U. 2009. Early detection of aging cartilage and osteoarthritis in mice and patient samples using atomic force microscopy. *Nature Nanotechnology,* 4**,** 186-192.

STOLZ, M., RAITERI, R., DANIELS, A. U., VANLANDINGHAM, M. R., BASCHONG, W. & AEBI, U. 2004. Dynamic elastic modulus of porcine articular cartilage determined at two different levels of tissue organization by indentation-type atomic force microscopy. *Biophysical Journal,* 86**,** 3269-3283.

STRUGLICS, A., OKROJ, M., SWÄRD, P., FROBELL, R., SAXNE, T., LOHMANDER, L. S. & BLOM, A. M. 2016. The complement system is activated in synovial fluid from subjects with knee injury and from patients with osteoarthritis. *Arthritis Research & Therapy,* 18**,** 1-11.

STYLIANOU, A., KONTOMARIS, S.-V., GRANT, C. & ALEXANDRATOU, E. 2019. Atomic Force Microscopy on Biological Materials Related to Pathological Conditions. *Scanning,* 2019**,** 1-25.

SUMBUL, F., MARCHESI, A., TAKAHASHI, H., SCHEURING, S. & RICO, F. 2018. High-Speed Force Spectroscopy for Single Protein Unfolding. *In:* LYUBCHENKO, Y. L. (ed.) *Nanoscale Imaging: Methods and Protocols.* New York City, New York, USA: Springer New York, 243-

264.
SUN, Y., WANG, T. L., TOH, W. S. & PEI, M. 2017. The role of laminins in cartilaginous tissues: from development to regeneration. *European Cells & Materials,* 34**,** 40-54.
TANAMAS, S. K., WLUKA, A. E., JONES, G. & CICUTTINI, F. M. 2010. Imaging of knee osteoarthritis *Gene Therapy,* 7**,** 635-647.
TOMKORIA, S., MASUDA, K. & MAO, J. 2007. Nanomechanical properties of alginate-recovered chondrocyte matrices for cartilage regeneration. *Proceedings of the Institution of Mechanical Engineers, Part H: Journal of Engineering in Medicine,* 221**,** 467-473.
TRAVASCIO, F. & JACKSON, A. R. 2017. The nutrition of the human meniscus: A computational analysis investigating the effect of vascular recession on tissue homeostasis. *Journal of Biomechanics,* 61**,** 151-159.
TSCHAIKOWSKY, M., BRANDER, S., BARTH, V., THOMANN, R., ROLAUFFS, B., BALZER, B. N. & HUGEL, T. 2022. The articular cartilage surface is impaired by a loss of thick collagen fibers and formation of type I collagen in early osteoarthritis. *Acta Biomaterialia,* 146**,** 274-283.
TSCHAIKOWSKY, M., SELIG, M., BRANDER, S., BALZER, B. N., HUGEL, T. & ROLAUFFS, B. 2021. Proof-of-concept for the detection of early osteoarthritis pathology by clinically applicable endomicroscopy and quantitative AI-supported optical biopsy. *Osteoarthritis Cartilage,* 29**,** 269-279.
VILLALVILLA, A., GÓMEZ, R., LARGO, R. & HERRERO-BEAUMONT, G. 2013. Lipid transport and metabolism in healthy and osteoarthritic cartilage. *International Journal of Molecular Sciences,* 14**,** 20793-20808.
VINCKIER, A. & SEMENZA, G. 1998. Measuring elasticity of biological materials by atomic force microscopy. *FEBS Letters,* 430**,** 12-16.
WANG, X. H., WEI, X. C., ZHANG, Q. Y. & CHEN, W. Y. 2007. Mechanical properties of chondrocytes isolated from normal articular cartilage: experiment with rabbit knees. *Zhonghua Yi Xue Za Zhi,* 87**,** 916-920.
WANG, Y., WLUKA, A. E., JONES, G., DING, C. & CICUTTINI, F. M. 2012. Use magnetic resonance imaging to assess articular cartilage. *Therapeutic Advances in Musculoskeletal Disease,* 4**,** 77-97.
WILUSZ, R. E., DEFRATE, L. E. & GUILAK, F. 2012. A biomechanical role for perlecan in the pericellular matrix of articular cartilage. *Journal of the International Society for Matrix Biology,* 31**,** 320-327.
WILUSZ, R. E., SANCHEZ-ADAMS, J. & GUILAK, F. 2014. The structure and function of the pericellular matrix of articular cartilage. *Journal of the International Society for Matrix Biology,* 39**,** 25-32.
WILUSZ, R. E., ZAUSCHER, S. & GUILAK, F. 2013. Micromechanical mapping of early osteoarthritic changes in the pericellular matrix of human articular cartilage. *Osteoarthritis and Cartilage,* 21**,** 1895-1903.
WOJDASIEWICZ, P., PONIATOWSKI, Ł. A. & SZUKIEWICZ, D. 2014. The role of inflammatory and anti-inflammatory cytokines in the pathogenesis of osteoarthritis. *Mediators of Inflammation,* 2014**,** 1-19.
XU, X., LI, Z., LENG, Y., NEU, C. P. & CALVE, S. 2016. Knockdown of the pericellular matrix molecule perlecan lowers in situ cell and matrix stiffness in developing cartilage. *Developmental biology,* 418**,** 242-247.
YANG, C. Y., CHANALARIS, A. & TROEBERG, L. 2017. ADAMTS and ADAM metalloproteinases in osteoarthritis - looking beyond the 'usual suspects'. *Osteoarthritis and cartilage,* 25**,** 1000-1009.
YOUN, I., CHOI, J. B., CAO, L., SETTON, L. A. & GUILAK, F. 2006. Zonal variations in the three-dimensional morphology of the chondron measured in situ using confocal microscopy.

Osteoarthritis and Cartilage, 14**,** 889-897.

ZELENSKI, N. A., LEDDY, H. A., SANCHEZ-ADAMS, J., ZHANG, J., BONALDO, P., LIEDTKE, W. & GUILAK, F. 2015. Type VI Collagen Regulates Pericellular Matrix Properties, Chondrocyte Swelling, and Mechanotransduction in Mouse Articular Cartilage. *Arthritis & Rheumatology* 67**,** 1286-1294.

ZHANG, L., LIU, G., HAN, B., WANG, Z., YAN, Y., MA, J. & WEI, P. 2020. Knee Joint Biomechanics in Physiological Conditions and How Pathologies Can Affect It: A Systematic Review. *Applied Bionics and Biomechanics,* 1**,** 1-22.

ZHANG, Z. 2015. Chondrons and the Pericellular Matrix of Chondrocytes. *Tissue Engineering Part B: Reviews,* 21**,** 267-277.

ZHAO, Z., LI, Y., WANG, M., ZHAO, S., ZHAO, Z. & FANG, J. 2020. Mechanotransduction pathways in the regulation of cartilage chondrocyte homoeostasis. *Journal of Cellular and Molecular Medicine,* 24**,** 5408-5419.

ZHENG, H. & CHEN, C. 2015. Body mass index and risk of knee osteoarthritis: systematic review and meta-analysis of prospective studies. *BMJ Open,* 5**,** 1-8.

Declaration of contributions

The study was carried out in the cell biology research laboratory, which is part of the university hospital for Orthopaedics, under the supervision of Prof. Dr. UK Hofmann and Ph.D. MSc M Danalache. Cartilage samples were obtained from the University Hospital of Tübingen and the Winghofer Medicum clinic in Rottenburg with help from PD Dr. M Schwitalle.

Prof. Dr. UK Hofmann and Ph.D. MSc M Danalache designed the study. Data acquisition occurred under the guidance of Ph.D. MSc M Danalache. Statistical analysis, processing and interpreting the collected data, including preparation of figures and tables and revision of the manuscript presented here, was carried out in consultation with Prof. Dr. UK Hofmann and Ph.D. MSc M Danalache.

I hereby declare that I have produced this work independently and have not used any source other than those listed in the bibliography. I affirm that any work from other authors is marked and referenced appropriately. The content of this thesis was published in the Journal of Biomechanics on December 3, 2019, by Danalache et al. and is used with the kind approval of the authors (Danalache et al., 2019a).

Acknowledgments

First, I would like to thank Prof. Dr. med. Ulf Krister Hofmann for introducing me to this topic and providing organizational and theoretical assistance in the course of the investigations.

I would also like to express my sincere gratitude for the extensive support of Ph.D. MSc Marina Danalache, who guided me through the project and was someone I could always count on. Further, I would also like to thank the other members of the orthopedics research group, which helped me in many ways and created a pleasant environment in which I carried out my research.

In addition, I would like to thank Prof. Gerd Klein, who gave me the possibility to use the AFM for the project.

I would also like to acknowledge the support from PD. Dr. med. Maik Schwitalle from the Winghofer Medicum for the supply of additional cartilage samples.

Lastly, I would like to thank my parents, whose support and motivation I can always rely on.